Journal of Controlled Release 253 (2017) 110–121

Contents lists available at ScienceDirect

Journal of Controlled Release

journal homepage: www.elsevier.com/locate/jconrel

Targeting ETS1 with RNAi-based supramolecular nanoassemblies for multidrug-resistant breast cancer therapy

Min Wu [a,b,1], Xingang Liu [a,1], Weihong Jin [b], Yongbing Li [a,b], Yang Li [a,b], Qinglian Hu [c], Paul K. Chu [b], Guping Tang [a,b,**], Yuan Ping [d,*]

[a] Institute of Chemical Biology and Pharmaceutical Chemistry, Zhejiang University, Hangzhou 310028, China
[b] Department of Physics & Materials Science, City University of Hong Kong, Tat Chee Avenue, Kowloon, Hong Kong, China
[c] College of Biotechnology and Bioengineering, Zhejiang University of Technology, Hangzhou 310032, China
[d] School of Materials Science and Engineering, Nanyang Technological University, Singapore 639798, Singapore

ARTICLE INFO

Article history:
Received 23 July 2016
Received in revised form 19 February 2017
Accepted 6 March 2017
Available online 14 March 2017

Chemical compounds studied in this article:
Adamantanecarboxylic acid (PubChem CID: 13235)
1,1′-Carbonyldiimidazole (PubChem CID: 68263)
Dimethyl sulfoxide (PubChem CID: 679)
Thiazolyl Blue (PubChem CID: 64965)
Triethylamine (PubChem CID: 8471)
Doxorubicin hydrochloride (PubChem CID: 443939)
DAPI (PubChem CID: 2954)
Acetic acid (PubChem CID: 176)
Sodium hydroxide (PubChem CID: 14798)
Ethanol (PubChem CID: 702)

ABSTRACT

Overexpression of erythroblastosis virus E26 oncogene homolog 1 (ETS1) gene is correlated with both tumor progression and poor response to chemotherapy in cancer treatment, and the exploitation of RNA interference (RNAi) technology to downregulate ETS1 seems to be a promising approach to reverse multidrug-resistant cancer cells to chemotherapy. Hence, the RNAi-based nanomedicine which is able to simultaneously downregulate ETS1 expression and to deliver chemotherapeutic agents may improve multidrug-resistant cancer therapy synergistically. In this study, we developed a supramolecular nanoassembly that could deliver siRNA targeting ETS1 (siETS1) and doxorubicin (DOX) as an effective nanomedicine to achieve successful chemotherapy towards multidrug-resistant breast cancer. The nanotherapeutic system was prepared by loading adamantane-conjugated doxorubicin (AD) into polyethyleneimine-modified (2-hydroxypropyl)-γ-cyclodextrin (HP) through the supramolecular assembly to form AD-loaded HP (HPAD), followed by electrostatically-driven self-assembly between siETS1 and HPAD. When the HPAD/siETS1 nanoassemblies were delivered into drug-resistant MCF-7/ADR cells, the drug efflux was significantly reduced as a result of simultaneous silencing of ETS1 and MDR1 genes. Importantly, the HPAD/siETS1 nanoassembly could enhance drug residence time at tumor site, and effectively inhibit drug-resistant tumor growth due to the inhibition of angiogenesis and necrosis in tumor tissues. Western blot analysis indicated that the gene expression of both ETS1 and MDR1 *in vivo* was considerably downregulated after the drug-resistant tumor-bearing mouse was treated with HPAD/siETS1 nanoassemblies. This study offers a new therapeutic delivery strategy targeting ETS1 for the effective multidrug-resistant chemotherapy.

Keywords:
Erythroblastosis virus E26 oncogene homolog 1
Nanomedicine
siRNA
Multidrug resistance
Doxorubicin
Drug delivery

1. Introduction

In spite of the advances in early diagnosis and treatment, successful breast cancer therapy remains to be a formidable challenge, because patients with breast cancer frequently develop simultaneous multidrug resistance (MDR) after long-term chemotherapy [1,2]. Many different mechanisms, including overexpression of multidrug resistance 1 (MDR1) gene which encodes P-glycoprotein (P-gp), drug inactivation,

* Correspondence to: Yuan Ping, School of Materials Science and Engineering, Nanyang Technological University, Singapore 639798, Singapore.
** Correspondence to: Guping Tang, Institute of Chemical Biology and Pharmaceutical Chemistry, Zhejiang University, Hangzhou 310028, China.
E-mail addresses: tangguping@zju.edu.cn (G. Tang), pingyuan7@gmail.com (Y. Ping).
[1] These authors contributed equally to this work.

http://dx.doi.org/10.1016/j.jconrel.2017.03.011
0168-3659/

alterations in drug targets, and DNA damage repair were responsible for MDR [3]. Among these mechanisms, overexpression of MDR1 had been the most widely studied [4]. Many recent studies had proved that the silencing of MDR-1 in multidrug-resistant cell lines could increase chemosensitivity to doxorubicin (DOX) *in vitro* [5–9]. Nevertheless, a variety of MDR-1 inhibitors failed to show significant clinical benefits, despite the evidence supporting the role for MDR-1 in MDR [10,11]. These facts explain that the diversity of ABC receptors, and only one specific efflux pump expression may be sufficient to induce drug resistance. As a result, it is urgent to develop new strategies and to find efficient new target to reverse drug resistance.

The erythroblastosis virus E26 oncogene homolog 1 (ETS1), which belongs to the member of the ETS family of transcription factors, is overexpressed in many types of cancer cells [12]. Experimental investigations show that ETS1 gene is involved in the drug resistance of ovarian, pancreatic, prostate cancer and breast cancer cells [13–16]. Intriguingly, the overexpression of ETS1 in multidrug-resistant human breast cancer cells was reported in recent years [17]. As a transcription factor, ETS1 regulates a number of genes coding for proteases such as matrix metalloproteinase (MMP1, MMP3 and MMP9) and urokinase type plasminogen activator (PLAU). These proteases are known to be involved in extracellular matrix (ECM) degradation which is required for the invasion of cancer cells [18,19]. As a result, ETS family members including ETS1 are known as candidate oncogenes, and the upregulation of multiple ETS factors is associated with metastasis and poor prognosis. Recently, the interaction between ETS1 and p53 was identified as one of the major mechanisms that can up-regulate the expression of MDR1 at the transcriptional level in drug-resistant human breast cancer cell lines [20]. Small interfence RNA (siRNA) targeting ETS1 was reported to effectively inhibit ETS1 gene expression, and significantly increase the sensitivity of multidrug-resistant breast carcinoma cells to adriamycin treatment *in vitro*. This suggests the delivery of siRNA targeting ETS1 is likely to enhance the efficacy of multidrug-resistant breast cancer chemotherapy *in vivo* [21].

To enhance the combination therapy efficacy *in vivo*, we herein propose a co-delivery strategy for the simultaneous delivery of ETS1 siRNA (siETS1) and DOX to accomplish combinational effects. The combination of chemotherapy and RNAi allows the administration of chemotherapeutic agents at lower doses, which potentially helps reduce side effects and improve therapeutic efficacy. As compare with monotherapy, the combination therapy exhibits better chemotherapeutic response and can improve survival rate [22,23]. The principle of this delivery strategy is based on the incorporation of an anticancer drug and an MDR modulator into the same nanoparticle, which allows the simultaneous delivery of two payloads into the same cancer cell population, thereby maximizing the therapeutic benefit. Recent studies mainly focused on targeting strategies [24,25] or stimuli-responsive delivery systems to enhance therapeutic efficiency [26]. For example, liposomal doxorubicin (L-DXR) functionalized with recombinant human E-selectin (ES) and polyethylene glycol (PEG) can target and kill cancer cells under shear flow [24]. Christian and co-workers used a integrated strategy to combine the feature of biological and physical drug targeting to trigger drug release and hyperthermia, which is primarily based on magnetic field influence for thermo-chemotherapy of cancers [26]. In addition to the above strategies, the simultaneous delivery of anticancer drugs and MDR inhibitors showed great promises to effectively inhibit tumor growth and invasion by improving the chemotherapeutic sensitivity. For example, the delivery of liposomes loaded with DOX (or paclitaxel) and P-gp siRNA appeared to be more cytotoxic to cancer cells than free drugs in combination of siRNA. So far, various co-delivery vectors including polymeric, liposomal, dendrimer [27], mesoporous silica [28] and cationic nanoparticles had been developed in the past few years [29–32]. In our recent studies, we showed that the co-delivery of anticancer drugs and siRNA *via* cycleodextrin-based supramolecular cationic polymers was more effective than the delivery of anticancer drugs and siRNA respectively [33–35]. In order to investigate whether the down-regulation of ETS1 would promote drug sensitivity and reverse MDR in breast cancer *in vivo*, we fabricated a supramolecular nanoassembly composed of polytheyleneimine-modified (2-hydroxypropyl)-γ-cyclodextrin (HP), 1-adamantane-conjugated DOX (AD), and siETS1 as a new type of nanomedicine for the multidrug-resistant breast cancer therapy. Hydrophobic AD was first loaded into hydrophobic core of γ-cyclodextrin of HP through supramolecular host-guest interaction to form AD-loaded HP (HPAD), and siETS1 was further complexed by the PEI arms of HP *via* electrostatic interaction (Scheme 1). As expected, the intracellular delivery of supramolecular nanoassemblies can significantly silence ETS1 and also reduced the protein expression levels of MDR1 to alleviate drug efflux, thereby resensitizing multidrug-resistant breast cells to chemotherapy. We also investigated the *in vivo* anti-tumor effect mediated by HPAD/siETS1 supramolecular assembly and further compared with a nanoassembly analog with MDR1 siRNA (siMDR1). We demonstrated that the HPAD/siRNA supramolecular nanoassembly exhibited increased therapeutic potential by inhibiting tumor angiogenesis and progression *in vivo*.

2. Materials and methods

2.1. Materials

Polyethyleneimine (branched PEI, MW 600 Da and 25 KD), 1-Adamantane Carboxylic Acid (Ada-COOH, MW 180.24), (2-Hydroxypropyl)-γ-cyclodextrin (γ-hy-CyD), ethanol, 1,1-carbonyldiimidazole (CDI), dimethyl sulfoxide (DMSO), [3-(4,5-dimethylthiazol-2-yl)-2,5-diphenyltetrazolium bromide] (MTT, MW 218.1), and triethylamine (TEA) were obtained from Sigma-Aldich (St. Louis, MO, USA). Doxorubicin hydrochloride (DOX·HCl) was purchased from Haida Pharmaceutical Co., Ltd. (Hangzhou, Zhejiang, China) and 4′,6-diamidino-2-phenylindole (DAPI) was bought from the Beyotime Institute of Biotechnology (Haimen, Jiangsu, China).

The negative control siRNA (siNC) and siRNA targeting green fluorescent protein (GFP-22) were purchased from Qiagen (Dusseldorf, Germany) and fluorescein-tagged negative-control siRNA (FAM-siRNA) was purchased from Biomics Biotechnologies Co., Ltd. (Nantong, Jiangsu, China). All other siRNAs were obtained from Shanghai Genepharma Co. Ltd. (China), including a double-stranded siRNA targeting ETS1 (sense, 5-ACUUGCUACCAUCCCGUAC-dTT-3′, antisense, 5-GUACGGGAUGGUAGCAAGU-dTT-3′) and a double-stranded siRNA targeting MDR1 (sense, 5-GACAGAAAGCUUAGU ACCA-dTT-3′, antisense, 5-UGGUACUAAGCUUUCUGUC-dTT-3′). The FITC-labeled P-gp and ETS1 antibody was supplied by eBioscience (San Diego, CA, USA).

2.2. Cells and animals

Human MCF-7 and MCF-7/ADR (DOX-resistant MCF-7 cell line) breast cancer cell line were obtained from the American Type Culture Collection (ATCC, MD, USA) and the MCF-7 cells with stable GFP expression (MCF-7/GFP) were provided by Prof. Jun Wang from University of Science and Technology of China, Hefei, China. The cells were cultured in RPMI1640 medium (GIBCO, Grand Island, NY, USA) supplemented with 10% fetal bovine serum (FBS), penicillin, and streptomycin at 37 °C in 5% CO_2 and MCF-7/ADR was maintained with free DOX at 1 μg/mL.

Athymic female mice (BALB/c strain) (4–5 weeks old, 16–18 g) were purchased from the Zhejiang Chinese Medical University and maintained in a pathogen-free environment under controlled humidity and temperature. The animal experiments were performed in accordance with the guidelines of China Animal Protection Law.

2.3. Synthesis and biochemical characterization of HPAD

γ-hy-CyD (1.622 g, 1.027 mmol) and CDI (1.70 g, 10.50 mmol) were dissolved in DMSO (10 mL), and were then mixed with 200 μL of TEA. The mixture was stirred at room temperature for 3 h under nitrogen.

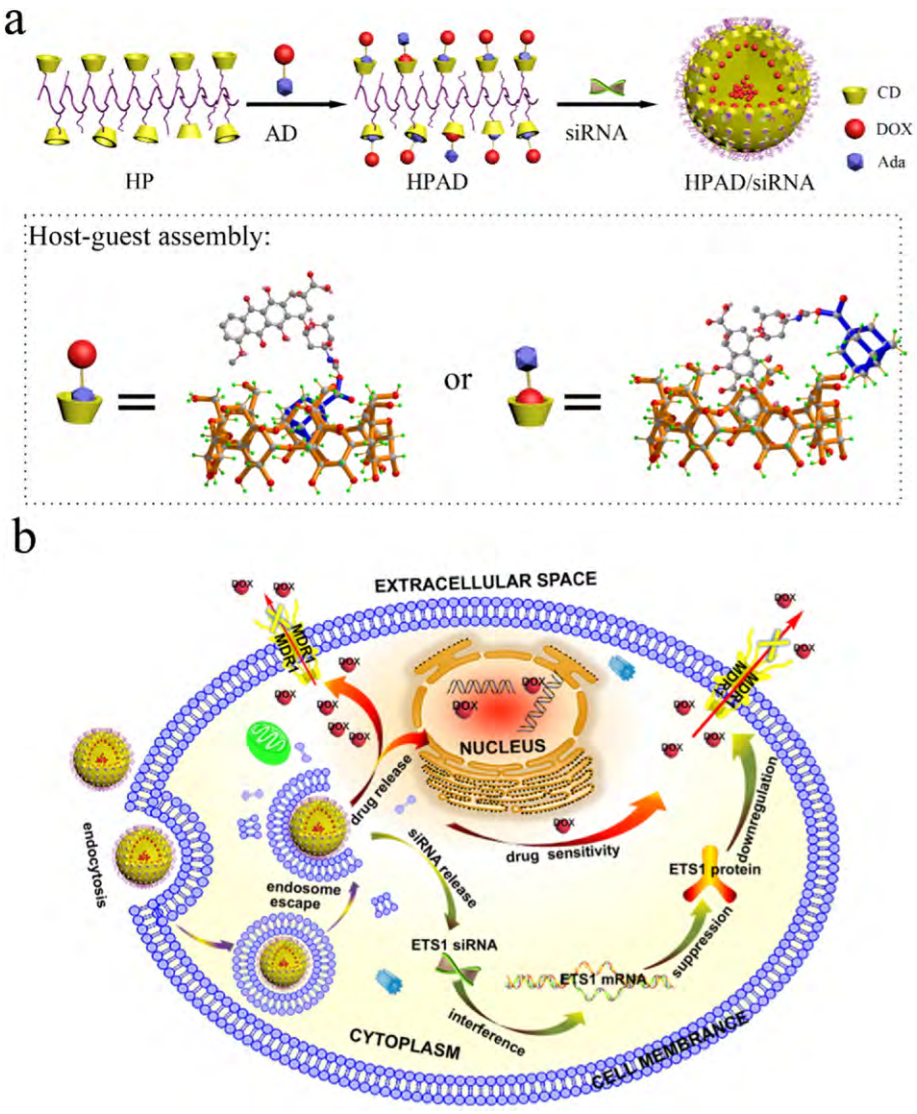

Scheme 1. (a) Schematic illustration of self-assembly process of supramolecular nanoassemblies HPAD/siRNA; (b) The intracellular delivery pathway of DOX-loaded, siRNA-complexed HPAD/siETS1 supramolecular nanoassemblies.

PEI (5.56 g, 9.27 mmol) was dissolved in DMSO (10 mL). After addition of TEA (200 μL), PEI solution was added dropwise to CyD-CDI over 2.5 h with stirring, followed by overnight reaction. The crude product was dialyzed in water for 2 days and freeze-dried for another 3 days.

HPAD conjugates were obtained by host-guest interaction. In brief, Ada-COOH (49.5 mg, 0.27 mmol) and CDI (48.1 mg, 0.30 mmol, 1.10 equiv) were dissolved in DMSO (2 mL), mixed with TEA (200 μL), and then stirred at room temperature for 24 h under nitrogen. Doxorubicin hydrochloride (105.0 mg, 0.19 mmol) dissolved in DMSO (2 mL) was slowly added to Ada-CDI and the mixture was further stirred overnight under nitrogen. Upon the addition of distilled water to remove excess CDI, γ-hy-PC (HP) (0.100 g) dissolved in H_2O (10 mL) were added dropwise to different amount of AD solutions (500 μL, 250 μL, 60 μL). The resultant mixture was stirred for 8 h. Then the crude product was dialyzed in water for 1 day and freeze-dried to yield red γ-hy-PC/AD (HPAD) powders.

The ^{1}H nuclear magnetic resonance (^{1}H NMR) and two-dimensional nuclear overhauser spectroscopy (2D-NOESY NMR) spectra of each sample were recorded on a BrukerDRX-400 spectrometer (Bruker, Ettlingen, Germany) at room temperature using DMSO-d_6 or D_2O as the solvent.

The particle size and zeta potential of the polymers were determined in triplicate at 25 °C by dynamic light scattering (DLS) on the Zetasizer Nano ZS (Malvern Instruments, Worcestershire, UK) with a laser light wavelength of 633 nm at a 173° scattering angle. The morphological properties of the nanoassemblies were examined by a Cambridge Stereoscan 260 scanning electron microscopy (SEM, Cambridge, UK), a Tecnai 10 transmission electron microscopy (TEM, Philips Electron Optics, Eindhoven, NL) and an atomic force microscopy (AFM, Auto Probe CP, Park Scientific Instruments).

2.4. pH-dependent drug release of DOX in vitro

The drug loading content was measured by a UV–vis spectrophotometer (UV-2800, Hitachi, Japan). 5.0 mg of the freeze-dried HPAD polymers were dissolved in 25 mL of DMSO and were assessed at λ = 480 nm. The calibration curve was established under the same conditions. The drug loading content (LC) of HPAD polymers for DOX was calculated by the following formula:

$$LC = (\text{mass of DOX encapsulated in micelles}/\text{mass of HPAD}) \times 100\%$$

The release of DOX from different loading content HPAD *in vitro* was monitored using the dialysis method. The HPAD nanoassemblies were dissolved in phosphate buffer solutions (PBS) at pH values of 5.0, 6.8 and 7.4, sealed in dialysis bags with a molecular weight cut-off of

8 kDa–14 kDa. The solutions were agitated on an orbital shaker at 100 rpm at 37 °C. At defined time intervals, the medium was removed and replenished by a fresh one. The amount of DOX released into the medium was determined was measured by UV Spectrophotometer (UV-3600, Shimazu, Japan) at the wavelength of 480 nm. The standard curves at different pH values were also established.

2.5. Cellular uptake investigation

The cellular uptake and distribution were examined by confocal microscopy. 5×10^4/well MCF-7/ADR cells were seeded onto 24-well plates and were grown for 20 h. 100 nM of FAM-siRNA was complexed with HP and NC-siRNA was complexed with HPAD at N/P 40 at room temperature for 20 min before use. After transfection for 4 h, the cells were fixed with fresh 4% paraformaldehyde and treated with DAPI for 10 min and cell nuclei were counterstained with DAPI (blue) and endolysosomes were stained by LysoTracker Green and LysoTracker Red, respectively. The images were acquired on a confocal scanning laser microscope (CLSM, Radiance 2100, Bio-Rad).

GFP-expressing MCF-7 cells (MCF-7/GFP) were used as a model in the green fluorescent protein (GFP) silencing study. The HPAD/siRNA nanoassembly formation and delivery to cells were completed as described above using GFP targeted siRNA (siGFP) and negative control (NC-siRNA). GFP silencing was tested by confocal scanning laser microscope and flow cytometry (Beckman-Coulter, USA) after cell collection [36].

The accumulation of DOX in MCF-7/ADR cells can be observed by confocal microscope [37]. The MCF-7/ADR cells were seeded on 24-well plate at a density of 5×10^4 in 1640 medium containing 10% FBS for 20 h. The medium was then replaced by 1 mL of 1640 (serum free), DOX and HPAD, and incubated for 4 h at a DOX concentration of 5 μg/mL. After the medium was taken out, the cells were washed and were cultured with 1 mL fresh complete medium at defined time points. The DOX accumulation in the cells was measured by confocal microscopy and flow cytometry.

2.6. Inhibition of protein expression by the HPAD/siRNA nanoassemblies

Western blotting analysis was used in the analysis of the expression of EST1 protein and MDR1 protein in MCF-7 or MCF-7/ADR cell lines. The cell proteins were extracted after different treatments and the total protein was quantified by the BCA protein assay kit (Promega, USA). An equal amount of protein was separated on the SDS-PAGE, transferred onto the nitro-cellulose membrane, blocked, and incubated overnight with monoclonal antibodies against ETS1, MDR1 and GADPH. After washing, the membrane was incubated with the horseradish peroxidase-conjugated secondary antibody for 2 h at room temperature. The bands were visualized using the Westzol enhanced chemiluminescence kit (Intron, Sungnam, Korea) and the expression was normalized to the housekeeping gene expression.

2.7. The biological characterization of HPAD in vitro

The cytotoxicity of the HPAD was evaluated by the MTT assay. The MCF-7 and MCF-7/ADR cells were seeded into a 96-well microplates at a density of 8×10^3 cells in complete medium (200 μL) per well for 20 h separately. The medium was replaced with 200 μL of 10% serum-free with different concentrations of selected chemicals. After further incubation for 24 h or 48 h, the solutions were then replaced with 100 μL of the serum-free medium containing 0.5 mg/mL MTT and incubated for another 4 h. Finally, after removal of MTT medium the formazan crystals were dissolved in DMSO (100 μL) and measured spectrophotometrically on an ELISA plate reader (Model 550, Bio-Rad) at a wavelength 570 nm.

The relative cell growth (%) related to control cells cultured in the media without the chemicals was calculated by the following formula:

$$V\% = ([A]\text{experimental} - [A]\text{blank})/([A]\text{control} - [A]\text{blank}) \times 100\%$$

where V% is the cell viability (%), [A]experimental is the absorbance of the wells culturing cells treated with chemicals, [A]blank is the absorbance of media blanks, [A]control is the absorbance of the wells culturing cells without chemical treatment. The half-maximal inhibitory concentration (IC_{50}) was determined by fitting data to the following equation:

$$V\% = \frac{100}{1 + ([DOX]/IC_{50})^P} \times 100\%$$

where V% is the viability (%), [DOX] is the concentration (mg/mL) of the

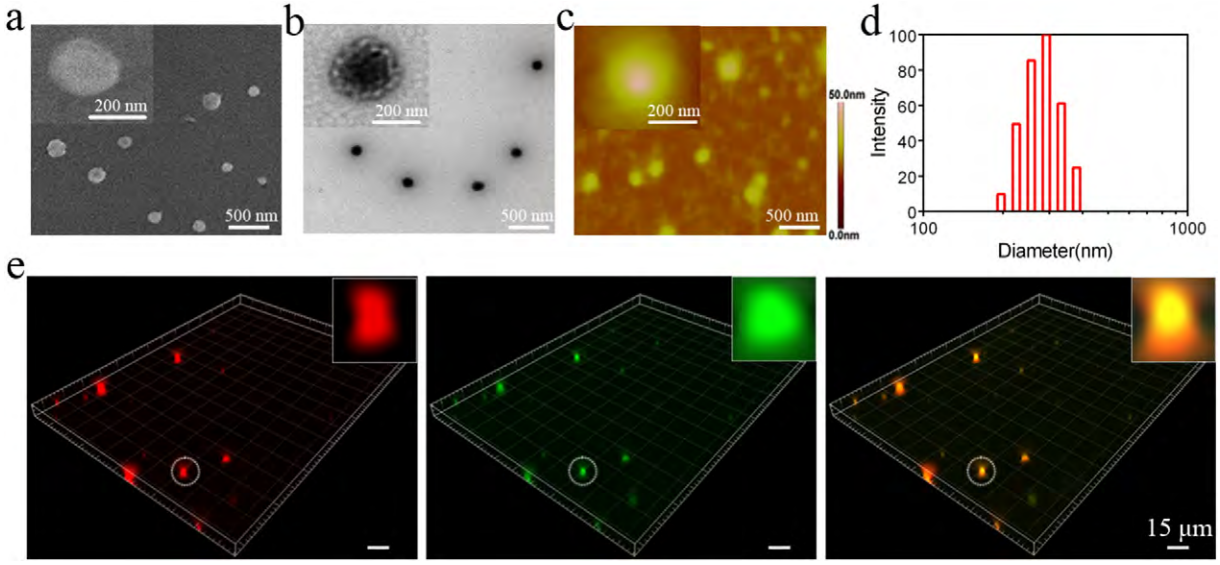

Fig. 1. (a) SEM image, (b) TEM image, (c) AFM image, (d) size distribution of HPAD/siRNA complexes at the N/P ratios of 40. (e) Re-constructed three-dimensional super-resolution microscopic images of HPAD/FAM-siRNA. Each grid in the left panel represents 1 × 1 μm. Green colour represents FAM-siRNA and red colour represents DOX-loaded HPAD. The yellow colour represents the merged fluorescence of DOX and FAM-siRNA.

DOX or equivalent DOX in HPAD at a well, and p was defined as the slope of the sigmoid curve.

2.8. In vivo tumor growth and survival rate assessment

Briefly, MCF-7/ADR cell lines were injected subcutaneously (100 μL injection volume, 1×10^7 cells) at the right abdominal of 5-weeks-old female BALB/c nude mice. The mice were used for *in vivo* fluorescence image when the tumors reached a size of approximately 100 mm^3 (about 2–3 weeks).

BALB/c nude mice bearing MCF-7/ADR breast tumors were randomly assigned to five groups and treated with the PBS, DOX, HPAD/NC-siRNA, HPAD/siETS1 and HPAD/siMDR1 when the tumor volume reached around 100 mm^3 two weeks after tumor inoculation. Each group consisted of eight mice (n = 8). The doses of siRNA of each intra-tumor injection were fixed at 0.6 mg/kg and the equivalent dose of DOX was 0.5 mg/kg. The treatment was performed twice a week for 2 weeks and the tumor growth was monitored using calipers twice a week. T tumor volume was calculated as: V (mm^3) = π/6 × length (mm) × $width^2$ (mm). Three mice from each group were sacrificed 30 Days later after first injection. Their tumors were dissected, weighed,

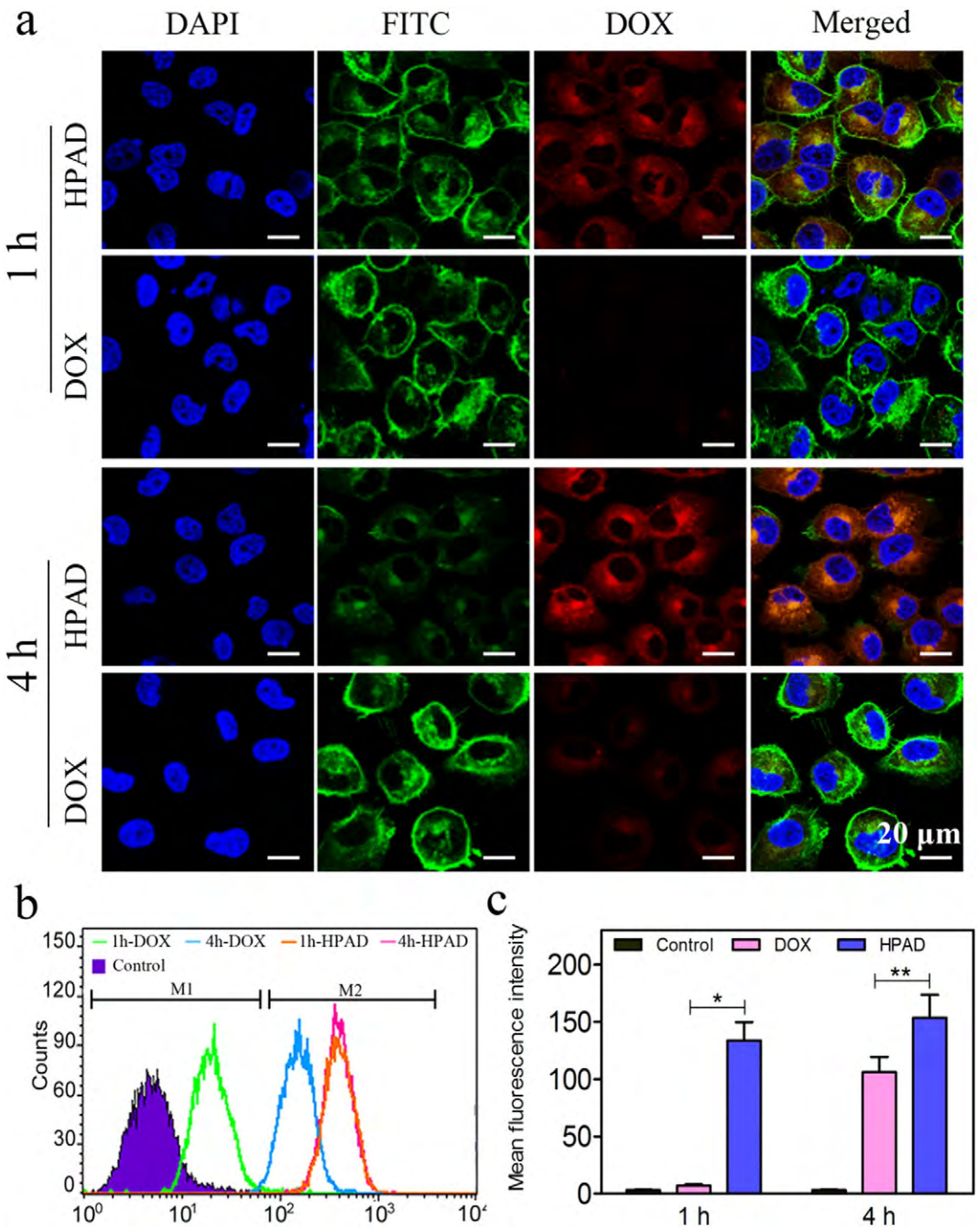

Fig. 2. (a) CLSM images of MCF-7/ADR cells incubated with free DOX or HPAD for 1 h or 4 h. The cells were counterstained with DAPI (blue) for the cell nucleus and Alexa Fluor 488 phalloidin (green) for the cell membrane. (b) Flow cytometry analysis and (c) relative fluorescence intensity of DOX in MCF-7/ADR cells incubated with free DOX or HPAD for different time. The equivalent dose of DOX was 5 μg/mL (n = 3, Student's *t*-test, *p < 0.05, **p < 0.01).

and then imaged. The other tumor-bearing mice were continuously observed for up to three months and differences in tumor growth were tested for statistical significance.

2.9. Immunohistochemical analysis of H&E, ETS1, MDR1, CD31 and TUNEL assay

In the histological assay, the paraffin-embedded tumor samples were cut into 5 mm thick sections, then dewaxed and rehydrated. After quenching endogenous peroxidase, achieving antigen retrieval and blocking non-specific binding sites, incubation with primary antibodies was carried out overnight at 4 °C. The antibodies used here were monoclonal ETS1 antibodies (concentration of 4–8 μg/mL) (polyclonal primary antibody, sc-1517, Abcam, USA), monoclonal antibody against MDR1 (concentration of 4–8 μg/mL) (Abcam, USA) and monoclonal anti-CD31 antibodies (1:200) (Beijing Biosynthesis Biotechnology Co., LTD). Biotinylated goat anti-rabbit antibodies were used as secondary antibodies at 1:200 for 30 min at room temperature. The samples were stained with hematoxylin and eosin (H&E) for microscopic observation. Apoptosis of the tumor cells was determined by the TUNEL method according to the manufacturer's instructions [38].

2.10. 2.10. Statistical analysis

All the experiments, where the obtained data were used for statistical analysis, were repeated at least three times and the data were expressed as means ± standard deviation. The statistical significance ($^{*}p < 0.05$ or $^{**}p < 0.01$) was evaluated by using student *t*-test when only two groups were compared. In all tests, statistical significance was set at $^{*}p < 0.05$, $^{**}p < 0.01$.

3. Results and discussions

3.1. Analysis of the relationship between ETS1 and MDR1 protein

We first tested whether the ETS1 and MDR1 proteins were overexpressed in MCF-7/ADR cells in comparison with non-multidrug-resistant MCF-7 cells. As shown in Figs. S1a and b, western blot analysis

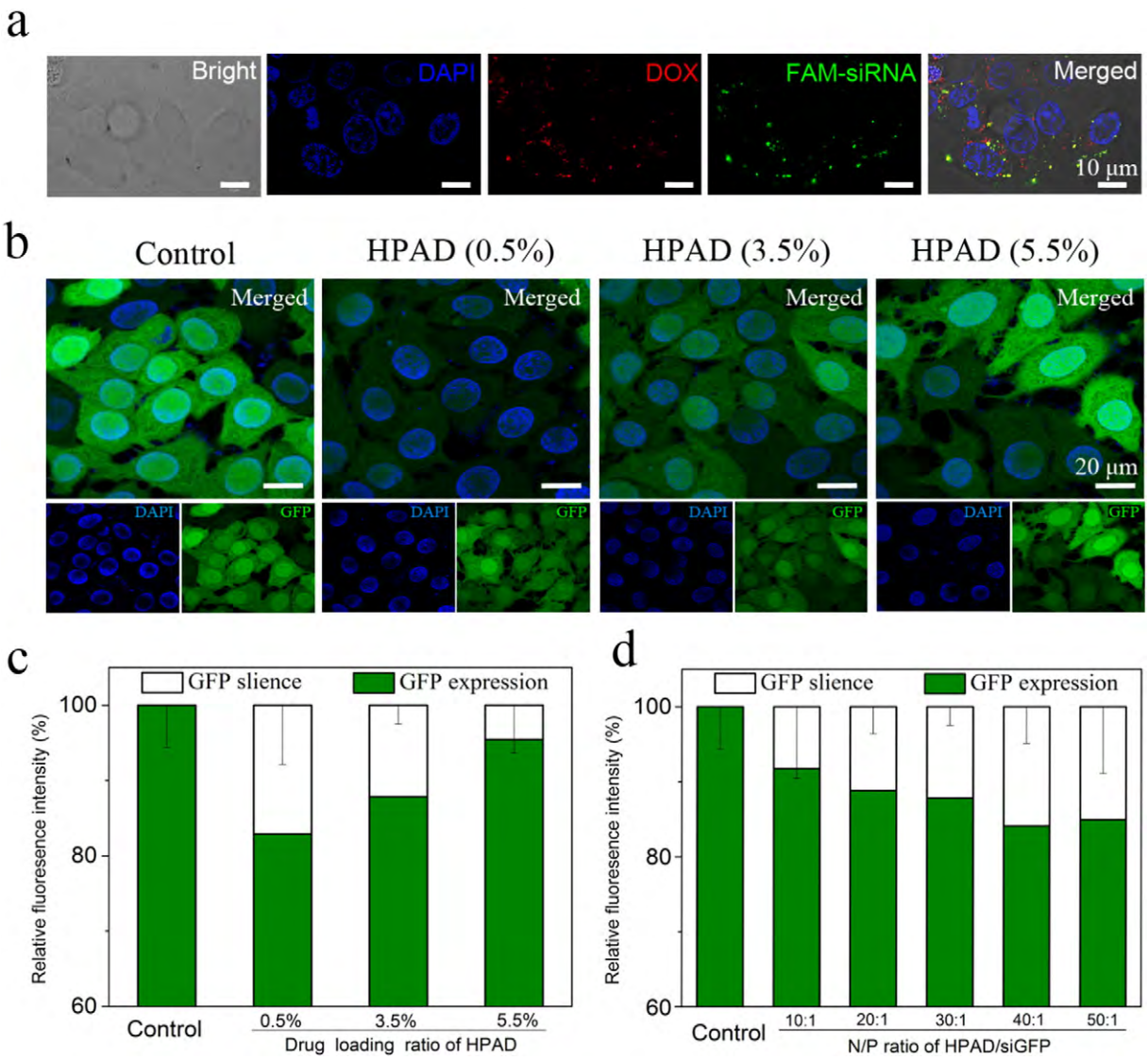

Fig. 3. (a) CLSM images of MCF-7/ADR cells incubated with HPAD/FAM-siRNA complexes for 4 h (DOX: red; FAM-siRNA: green; Nucleus: blue). (b) CLSM of MCF-7/GFP cells treated with HPAD/siGFP complexes to investigate the effect of drug loading ratio on GFP silencing efficiency. Relative silencing efficiency of GFP expression were determined by flow cytometry in MCF-7/GFP cells treated with HPAD/siGFP (c) with different loading of DOX and (d) with different N/P ratios.

confirmed that the levels of both ETS1 and MDR1 proteins expression were significantly higher in the MCF-7/ADR cells than those in the MCF-7 cells. The observation implied that there might be certain relationships between ETS1 and MDR1, both of which were probably associated with the MDR of breast cancer cells. We subsequently studied the protein-protein interaction (PPI) networks of ETS1 and MDR1 using STRING v10 software, a known database to predict PPI including direct (physical) and indirect (functional) associations [39]. As showed in Fig. S1c, the relationships of eight tumorigenesis-regulated proteins (ETS1, MDR1, MMP1, PLAU, BRCA1, P53, MAPK8 and CDKN1A) indicated that ETS1 play a key role in the PPI network. These observations clearly indicated that ETS1, as a transcription factor, may control the gene expression of multiple proteins which were related to tumor progression, and could be a new therapy target for MDR reversal. The co-delivery of DOX and siRNA targeting ETS1 may offer a possibility to inhibit tumor growth in multidrug-resistant cancer cell lines.

3.2. Preparation and characteristic of HPAD/siRNA NPs

Cyclodextrins had been studied extensively as a family of relatively simple host molecules, and served as drug carriers to deliver hydrophobic drugs. In our previous studies, low-molecular-weight polyethyleneimine (PEI) crosslinked by cyclodextrins (CyDs) were used as carriers to deliver both nucleic acids and hydrophobic drugs for cancer treatment, which showed low cytotoxicity and high efficiency in delivering these payloads both *in vitro* and *in vivo* [40,41]. As the hydroxyalkyl derivative of γ-cyclodextrin, (2-hydroxypropyl)-γ-cyclodextrin (γ-hy-CyD) exhibited a higher water solubility and could form stable complex with 1-adamantanecarboxylic acid, which possessed the high drug loading capacity of adamantine-modified hydrophobic drugs, such as adamantly doxorubicin (AD), and improved the water solubility of DOX [42]. In this work, firstly the HP self-assembled with AD to form supramolecular inclusion complexes HPAD, which was then complexed with siRNA to obtain HPAD/siRNA nanoassemblies.

To identify the molecular structure and the supramolecular interaction between AD and HP, ^{1}H nuclear magnetic resonance (^{1}H NMR) and two-dimensional nuclear Overhauser effect spectroscopy NMR (NOESY) spectra of HPAD were showed in Fig. S2. In the ^{1}H NMR spectrum of HPAD (Fig. S2a), the signals between 7.6 and 8.1 ppm were assigned to protons on the aromatic rings of DOX, the multiplets between 1.5 and 2.0 ppm were assigned to the protons of adamantyl moieties, whereas the multiplets between 2.3 and 2.8 ppm were assigned to the methylene protons of PEI, and the characteristic peak at 1.1 ppm was ascribed to methyl group of HP. As showed in the NOESY spectrum in Fig. S2b, the proton signals of adamantyl moieties (blue area) and anthraquinonic moieties (red area) were well correlated with the inner protons of HP (yellow area), indicating the successful host–guest inclusion complexation between HP and AD.

The size and morphology of supramolecular nanoassemblies were examined by SEM, DLS, TEM and AFM. As shown in Fig. 1a–d, the HPAD/siRNA nanoassemblies exhibited spherical morphology with the average size of 250 ± 30 nm. It was noted that the particle size generally increased with the N/P ratio, reaching c.a. 350 nm at N/P ratio of 40 (Fig. S3a). The zeta potential stabilized in the range of + (40–50) mV, indicating that the surface charge of HPAD/siRNA nanoassemblies was less influenced by N/P ratio (Fig. S3b). The confocal images of HPAD/FAM-siRNA nanoassemblies in Fig. 1e indicated the co-localization of the inherent red fluorescence of DOX with the green fluorescence of

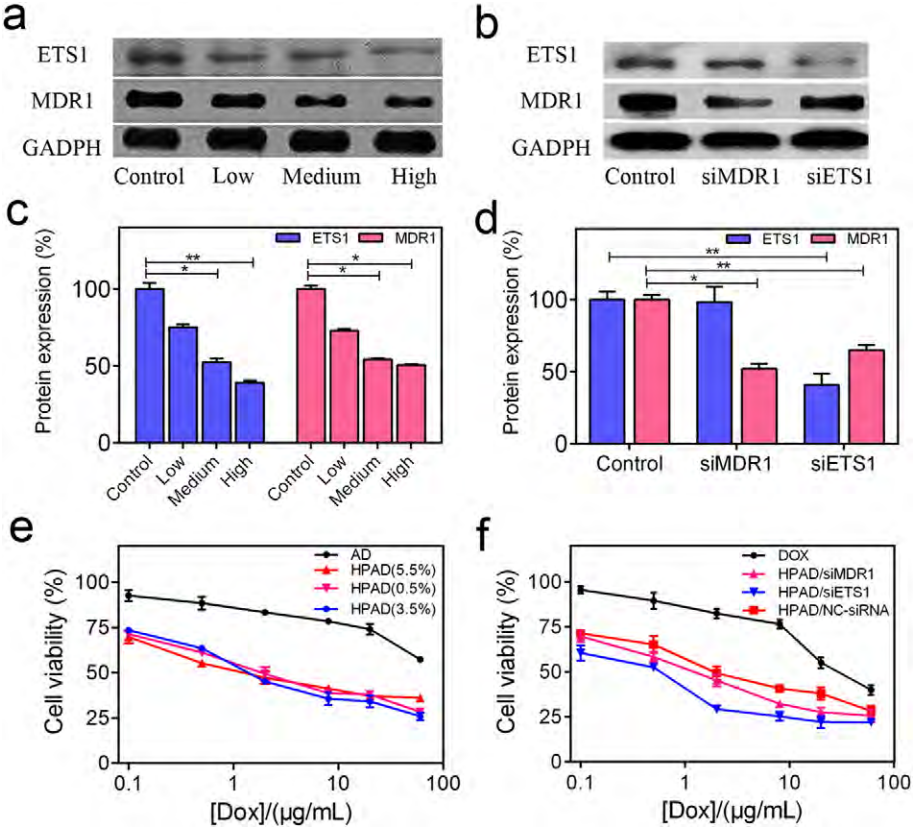

Fig. 4. Western blot analysis of ETS1 and MDR1 expression for MCF-7/ADR cells treated with different formulations. (a) MCF-7/ADR cells treated with HPAD/siETS1 complexes with different dose of siETS1 (Low: 10 nM, Medium: 20 nM, High: 30 nM). (b) MCF-7/ADR cells treated with different kind of HPAD/siRNA complexes. (siMDR1 and siETS1 represent HPAD/siMDR1 and HPAD/siETS1 respectively. (c) The relative expression of ETS1 and MDR1 protein treated with different dose of siETS1. (d) The relative expression of ETS1 and MDR1 protein treated with different kind of HPAD/siRNA complexes. (e) Cell viability of MCF-7/ADR cells after the treatment with HPAD with different DOX loading efficiency for 48 h. (f) Cell viability of MCF-7/ADR cells after the treatment with free DOX, HPAD/NC-siRNA, HPAD/siETS1 and HPAD/siMDR1 for 48 h. All data represent mean ± SD (n = 3). (Student *t*-test, *p < 0.05, **p < 0.01).

Table 1
Values of IC50 [equivalent to DOX] treated with various formulations.

Compounds	DOX	HPAD/NC-siRNA	HPAD/siETS1	HPAD/siMDR1
IC50 (μg/mL)	42.5	12.8	5.2	8.2

the FITC-labeled siRNA. The overlap of both signals yielded yellow fluorescence, suggesting the successful encapsulation of DOX and siRNA by HP. The positive charge and suitable particle size of the HPAD/siRNA nanoassemblies made it suitable for the efficient cellular uptake by cancer cells.

The drug release kinetics of DOX from HPAD *in vitro* was also studied. The release behavior was investigated at pH 7.4, 6.8 and 5.0 to mimic the normal physiological environment, the mildly acidic condition in tumor tissues, and the acidic endo/lysosomes, respectively. As showed in Fig. S4, all three HPAD with different drug loading efficiency (0.5%, 3.5%, and 5.5%) released DOX in a time- and pH-dependent manner. In general, the fast release DOX from HPAD in the acidic pH, whereas 13–25% of the total encapsulated DOX was slowly released from the HPAD nanoassemblies within 84 h. The accelerated DOX release in the acidic pH is attributed to the dissociation of adamantane-conjugated DOX (AD) from the cyclodextrin cavity, since DOX become more hydrophilic in the acid environment [43], and in turn decreases the supramolecular interaction force with HP. The difference in drug release kinetics at extracellular physiological pH and endosomal/tumoral pH conditions intracellular is advantageous for the delivery and the release of DOX to tumor sites and intracellular endosomal environments with minimal pre-mature release, which ensures the effective cytotoxicity against cancer cells. Using AD instead of DOX as the guest drug molecule, we find such an approach provides the advantages of controlled modular drug loading and minimizes the premature drug release, as the adamantyl moiety may facilitate DOX to form a more stable inclusion complexes with HP.

3.3. Synergistic effects of siETS1 and DOX in vitro

The MCF-7/ADR cell line was a type of DOX-resistant breast cancer cell line with low uptake level of free DOX, and it overexpressed ATP-binding cassette (ABC) transporters which were known to be associated with MDR [44]. The MCF-7/ADR cell uptake of HPAD loaded with 3.5% DOX was examined by confocal laser scanning microscopy (CLSM). As shown in Fig. 2a, MCF-7/ADR cells treated with HPAD for either 1 h or 4 h showed higher intracellular accumulation of DOX than those treated with free DOX, which was also assessed by quantitative analysis of DOX fluorescence intensity with flow cytometry (Fig. 2b, c). The above results indicated that HPAD could enhance the cell uptake of DOX by MCF-7/ADR cells, which were consistent with previous reports that nanocarrier-mediated drug delivery may bypass drug efflux pumps [45].

In order to further investigate the intracellular delivery of siRNA and DOX into MCF-7/ADR cells, cellular uptake of HPAD/FAM-siRNA nanoassemblies by MCF-7/ADR cells were visualized by CLSM. As showed in Fig. 3a, the fluorescence of DOX and FITC-labeled siRNA co-localize in the cytoplasm of MCF-7/ADR cells. More specifically, these HPAD/FAM-siRNA nanoassemblies were found to accumulate in the endo/lysosomes as well as over the cell membranes (Figs. S5, S6). The above results suggest that the supramolecular nanoassemblies are able to efficiently co-deliver drug and siRNA into a single cell efficiently, partly may due to the minimum drug efflux effect.

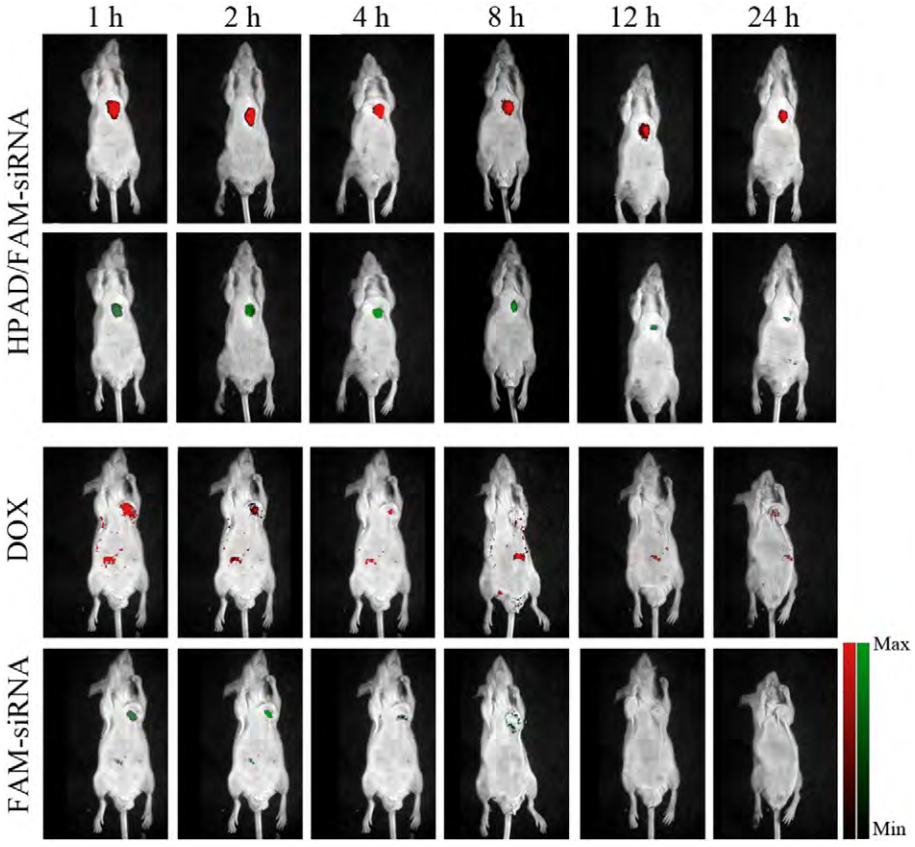

Fig. 5. Time-dependent *in vivo* fluorescence images of MCF-7/ADR tumor-bearing mouse treated with HPAD/FAM-siRNA complexes (10 μg FAM-siRNA, N/P = 40, 20 μL) or free DOX (90 μg, 20 μL) or free FAM-siRNA (10 μg, 20 μL). Images were taken at 1, 2, 4, 8, 12, and 24 h after the intratumoral injection by *In-vivo* Imaging System FX Pro, Kodak, USA. (Red and green colour represented the fluorescence signals of DOX and FAM-siRNA respectively).

RNA interference (RNAi) takes the advantage of the ability of siRNA to produce the specific degradation of complementary mRNA sequences, inhibit translation and specifically down-regulate the expression of the target protein [46]. To investigate the gene silencing efficiency of the HPAD/FAM-siRNA nanoassemblies *in vitro*, we chosen the MCF-7 cell line stably expressing green fluorescent protein (MCF-7/GFP) to evaluate the GFP protein silencing efficiency. The down-regulated expression of GFP was detected by flow cytometry and confocal laser scanning microscopy. As shown in Fig. 3d, the gene silence efficiency was largely dependent on N/P ratio, and the highest silence efficiency was achieved when N/P ratio was 40. At the N/P ratio of 40, the drug loading amount in nanoassemblies may also affect the silence efficiency. As shown in Fig. 3b and S7, GFP expression in MCF-7/GFP cells was downregulated when the siRNA delivery was mediated by HPAD. The GFP silencing efficiency of HPAD (for both 0.5% and 3.5% groups) was about 15% (Fig. 3c), which was close to the previous reports that 20–26% GFP silencing efficiency was achieved with lipid-modified PEI [36]. The reduced silencing efficiency was probably due to the decreased colloidal stability of HPAD induced by strong hydrophobic interactions. In order to balance the silence efficiency and drug loading amount, we decide to choose the HPAD group with the drug loading amount of 3.5% in the subsequent investigations.

We then investigated the effects of the HPAD/siETS1 nanoassemblies on ETS1 expression in MCF-7/ADR cells. Firstly, the effect of serum on cellular uptake was examined. In the presence of 10% serum, the cellular uptake of HPAD/FAM-siRNA nanoassemblies was only about 60% (in terms of DOX fluorescence intensity) as compared to that in the absence of serum (Fig. S9), probably owing to the interaction between HP and serum proteins. This suggests that the uptake process should be carried out in the serum-free condition instead to enhance cellular uptake efficiency [47,48]. Next, we investigated the ability of HPAD to deliver siRNA *in vitro*. As depicted in Fig. S8, HPAD/FAM-siRNA nanoassemblies was internalized by MCF-7/ADR cells, and reached a FITC-positive cell population of 78%. However, only 5% of total cell population was FITC-positive in the case of free siRNA, which suggest that HPAD facilitate the intracellular delivery of siRNA efficiently. Finally, we examined the optimal siRNA dose that is required for the effective knockdown of ETS1 expression in MCF-7/ADR cells. As shown in Fig. 4a, the gene silencing of ETS1 protein levels was dose-dependent, and the most effective inhibition of ETS1 protein expression mediated by HPAD/siETS1 was achieved at the dose of 30 nM siETS1, reaching 60% ETS1 protein knockdown in MCF-7/ADR cell lines (Fig. 4c).

At last, we compared the protein knockdown efficiency of siETS1 and siMDR1. As showed in Fig. 4b, d, the optimal siRNA dose induced 60% and 35% knockdown efficiency of ETS1 and MDR1 protein expression in HPAD/siETS1 group respectively, while there was negligible knockdown of ETS1 protein expression in HPAD/siMDR1 group. The above results suggest the potential of HPAD/siETS1 nanoassemblies in

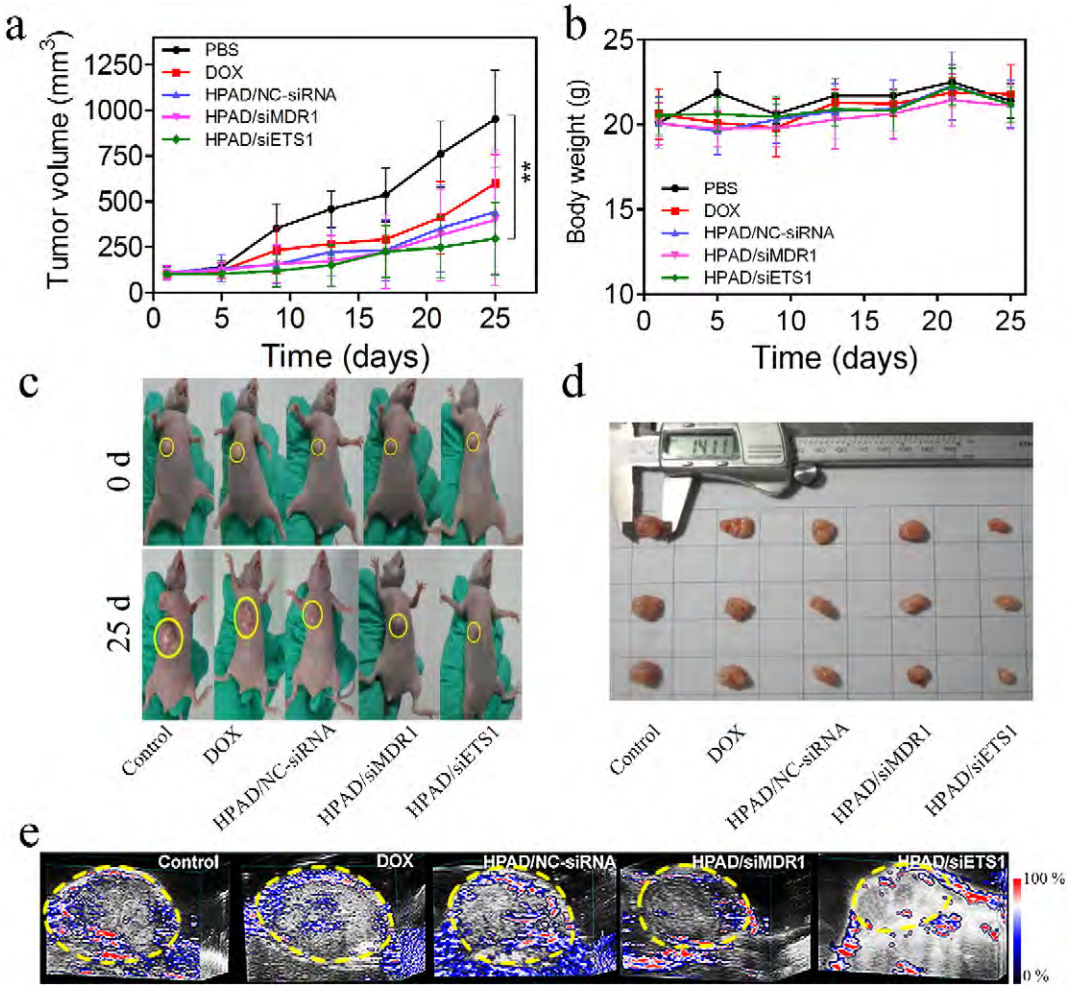

Fig. 6. *In vivo* therapeutic efficiency of HPAD/siRNA complexes. BALB/c nude mice with MCF-7/ADR xenografts were treated with HPAD/siMDR1, HPAD/siETS1 and other formulations. (a) Tumor volume and (b) the average body weight changes were measured every four days. Data represent mean ± SD (n = 6, Student's *t*-test, $^{**}p < 0.01$). (c) Images of *in vivo* tumor growth on 0 day and 25 day and (d) dislodged tumors from the mice after the last injection. (e) *In vivo* photoacoustic images of oxygen saturation (sO_2) in tumor tissues 25 day after the first treatment. Red and blue signals represented oxygenated and hypoxic regions, respectively. The yellow dash line indicated the tumor region identified by ultrasound image.

the effective down-regulation of both the ETS1 and MDR1 protein levels at cellular lever. The impressive dual inhibition function of siETS1 may be of paramount importance in MDR cancer therapy, since ETS1 protein plays an important role in angiogenesis and anti-apoptosis [17] and the overexpression of MDR1 protein is well known for promoting drug efflux in multidrug-resistant cancer cells [49]. We further evaluated the anti-proliferation efficiency of HPAD with different DOX loading amount in MCF-7 and MCF-7/ADR cells. In MCF-7/ADR cells, the antiproliferation effect of HPAD was much higher than that of adamantly doxorubicin (AD), which was probably due to the multidrug resistance phenotype of MCF-7/ADR cells (Fig. 4e). In MCF-7 cells, however, free AD showed a higher antiproliferation effect than HPAD at the concentration of 10 μg/mL, indicating the important role of HP for evading dug efflux (Fig. S10).

Next, the cytotoxicity of free DOX, HPAD, HPAD/siETS1 nanoassemblies and HPAD/siMDR1 nanoassemblies against MCF-7/ADR cells were evaluated (Fig. 4f). In general, whereas free DOX only showed mild cytotoxicity from 0.1–8 μg/mL, HPAD was able to induce much higher cytotoxicity compared with the equivalent free DOX. After complexing siETS1 with HPAD, the resulted HPAD/siETS1 nanoassemblies exhibit more cytotoxic than HPAD/siMDR1 at the equivalent DOX dose of 2 μg/mL. As shown in Table 1, the calculated half-maximal inhibitory concentration (IC_{50}) value follows the following order: HPAD/siETS1 < HPAD/siMDR1 < HPAD < DOX. The enhanced cytotoxicity of HPAD/siETS1 over other groups may contribute to the enhanced ETS1-associated cell apoptosis and the reduced drug efflux effect.

3.4. Combined therapeutic effect of siETS1 and DOX in vivo

The above promising results stimulated us to further explore whether DOX and siRNA can effectively reside within tumor after the intratumoral injection of HPAD/siETS1 nanoassemblies. Fig. 5 revealed time-dependent *in vivo* fluorescence images of BALB/c nude mice with

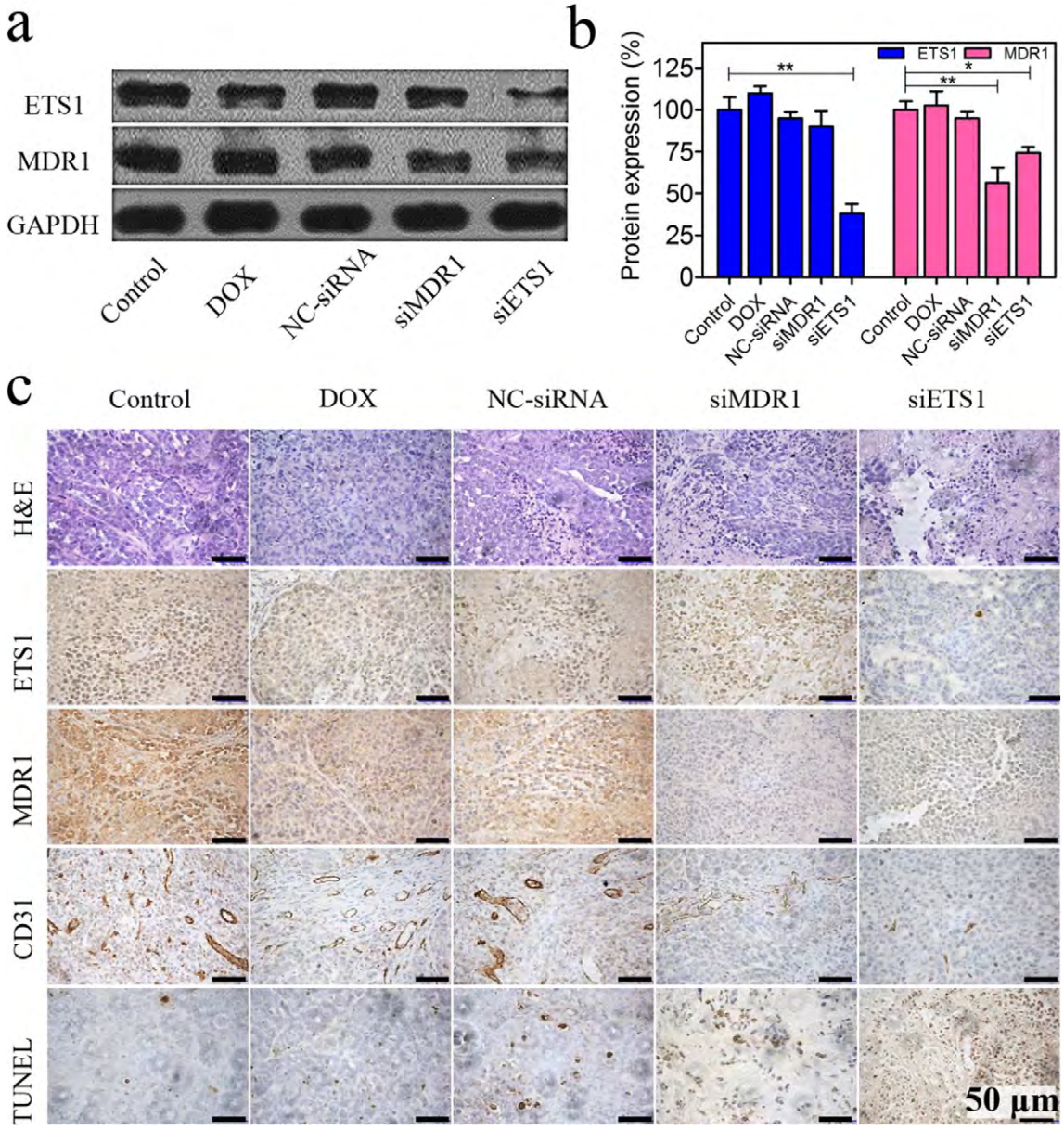

Fig. 7. (a) Western blot analysis of ETS1 and MDR1 expression in MCF-7/ADR tumors after the last treatment with different formulation *in vivo*. (b) The relative expression of ETS1 and MDR1 protein. The ratio of ETS1 and MDR1 to GADPH protein was calculated respectively. Data represent mean ± SD (n = 3). (Student *t*-test, $^{*}p < 0.05$, $^{**}p < 0.01$). (c) Immunohistochemical analyses of H&E, ETS1 protein, MDR1 protein, CD31 and TUNEL for MCF-7/ADR tumor tissues after the last treatment with different formulation *in vivo*. (NC-siRNA, siMDR1 and siETS1 represent HPAD/ NC-siRNA, HPAD/ siMDR1 and HPAD/ siETS1 respectively).

MCF-7/ADR xenografts after the intratumoral injection of HPAD/FAM-siRNA nanoassemblies or free DOX or free FAM-siRNA. As expected, in the case of free DOX group, the red fluorescence signals in the tumor site decreased dramatically with time, becoming negligible after 12 h post-injection. The quick clearance of free DOX from the body may probably due to the drug efflux of MDR, which resulted in relatively short residence time at tumor site. To the free FAM-siRNA group, similar quick clearance behavior were also observed, which is probably owing to the instability of free siRNA *in vivo*. In contrast, for HPAD/ FAM-siRNA group, despite the gradually faded fluorescence signals in tumor site, strong fluorescence intensity of DOX and FAM-siRNA still could be acquired even at 24 h post-injection. This demonstrates that HPAD/siRNA nanoassemblies can protect the siRNA from degradation and enhance the DOX retention within the tumor site, which may significantly facilitate drug and siRNA delivery efficiency *in vivo*.

Furthermore, we explored whether the synergistic anticancer effect could be achieved *in vivo*. Antitumor treatments were performed when tumors grew up to 100 mm^3, and five groups of mice were treated with PBS, free DOX, HPAD, HPAD/siMDR1 and HPAD/siETS1 respectively. The tumor volumes and body weights were measured every 4 days up to a total of 25 days. Although all the treatment groups showed certain extent therapeutic effects compared with the control group (Fig. 6a), the most effective therapeutic effect was achieved in group treating with HPAD/siETS1 nanoassemblies (Fig. 6c, d). In addition, no obvious influence were found on the average body weight of the mice that were treated with these formulations, indicating negligible side effect of the supramolecular nanoassemblies for antitumor therapy at the defined dose (Fig. 6b).

In vivo photoacoustic images of oxygen saturation (sO_2) were also assessed in the tumor tissues 25 days after the first treatment [50,51]. As shown in Fig. 6e, red and blue signals represent oxygenated and hypoxic regions, respectively. There was significant difference between the HPAD/siETS1 group and other groups in terms of sO_2 mapping, which may be attributed to the function of siETS1 in inhibiting angiogenesis in the tumor tissues. As depicted in Fig. 6e, the tumor volume in the mice treated with HPAD/siETS1 was much smaller compared to other groups. The results of western blots were also in good agreement with those *in vitro* data, suggesting the same mechanism of HPAD/siETS1 nanoassemblies in down-regulating ETS1 and MDR expression *in vivo* (Fig. 7a, b). From those results above, we can conclude that the siETS1 down-regulated gene expression of ETS1 and MDR1 leads to the enhancement of the drug sensitivity and apoptosis in the tumor cells *in vivo*.

Previous studies had showed that ETS1 expression was correlated with the specific features of gastric [52], renal [53], and hepatocellular carcinoma cells [54,55] including tumor histological differentiation, invasion, and metastasis. We assumed that these features might be the reason behind the more effective anti-tumor effect mediated by HPAD/siETS1 nanoassemblies. To confirm our hypothesis, we tested the cell apoptosis and angiogenesis in the tumors after treatment by histological examination (Fig. 7c). The H&E stained sections of tumor tissues from PBS and free DOX groups appeared to be most hypercellular and showed more obviously the nuclear polymorphism. Among these therapeutic groups, the tumor tissues from the treatment with the HPAD/siETS1 formulation showed the fewest tumor cells and the highest level of tumor necrosis. Immunohistochemical assays were performed to detect ETS1 and MDR1 expression in tumor tissues of mice after the different treatments. Cell nuclei were stained blue and the brown blots indicated the ETS1 or MDR1 protein in the tumor tissue. A distinct decrease in protein density in the tumor slice was observed after the treatment with HPAD/siETS1 nanoassemblies, which is in contrast with other treatment groups. The results are similar to that of western blot *in vitro* and *in vivo*. Microvessel density, as determined by immunohistochemical analysis with the blood vessel endothelial cell marker CD31, was significantly lower when the mouse was treated by HPAD/siETS1 nanoassemblies. The TUNEL assay also showed that the treatment with the formulation of HPAD/siETS1 could induce much more TUNEL-positive cells. These results of antitumor efficacy of HPAD/siETS1-based treatment further validate the effectiveness of the supramolecular nanoassembly formulation for the treatment of multidrug-resistant tumor in murine models *in vivo*.

4. Conclusion

In conclusion, we developed a supramolecular nanoassembly as the new nanomedicine for the effective RNAi against ETS1 and the efficient delivery of chemotherapeutic agents to improve multidrug-resistant cancer therapy. Whereas the nanoscaled dimension and the positive surface charge allows the HPAD/siETS1 nanoassemblies to be efficiently internalized by MCF-7/ADR cells, the RNAi induced by the supramolecular assembly is able to down-regulate both EST1 and MDR1 gene expression to prevent drug efflux. In the drug-resistant tumor-bearing mouse model, the intratumoral injection of HPAD/siETS1 nanoassemblies resulted in enhanced drug residence time at tumor site, as well as efficacious tumor suppression, largely owing to the necrosis and inhibition of angiogenesis in tumor tissues. In agreement with western blot analysis *in vitro*, the gene expression of both ETS1 and MDR1 *in vivo* were also significantly down-regulated after the mouse was treated with HPAD/siETS1 nanoassemblies. The success of this therapeutic strategy defines a unique modality for the effective multidrug-resistant cancer therapy in the dawning era of personalized nanomedicine.

Acknowledgments

This work was jointly supported by National Basic Research Program (2014CB931900), City University of Hong Kong Applied Research Grant (ARG) Nos. 9667066 and 9667069, Hong Kong Research Grants Council (RGC) General Research Funds (GRF) Nos. 112510 and 112212.

Appendix A. Supplementary data

Supplementary data to this article can be found online at http://dx.doi.org/10.1016/j.jconrel.2017.03.011.

References

[1] M.M. Gottesman, V. Ling, The molecular basis of multidrug resistance in cancer: the early years of P-glycoprotein research, FEBS Lett. 580 (2006) 998–1009.
[2] J.T. Sims, S.S. Ganguly, H. Bennett, J.W. Friend, J. Tepe, R. Plattner, Imatinib reverses doxorubicin resistance by affecting activation of sTAT3-dependent NF-kappa B and HSP27/p38/AKT pathways and by inhibiting ABCB1, PLoS One 8 (2013), e55509.
[3] C.F. Higgins, Multiple molecular mechanisms for multidrug resistance transporters, Nature 446 (2007) 749–757.
[4] M.M. Gottesman, T. Fojo, S.E. Bates, Multidrug resistance in cancer: role of ATP-dependent transporters, Nat. Rev. Cancer 2 (2002) 48–58.
[5] H. Meng, M. Liong, T. Xia, Z. Li, Z. Ji, J.I. Zink, A.E. Nel, Engineered design of mesoporous silica nanoparticles to deliver doxorubicin and P-glycoprotein siRNA to overcome drug resistance in a cancer cell line, ACS Nano 4 (2010) 4539–4550.
[6] M. Nourbakhsh, M.R. Jaafari, H. Lage, K. Abnous, F. Mosaffa, A. Badiee, J. Behravan, Nanolipoparticles-mediated MDR1 siRNA delivery reduces doxorubicin resistance in breast cancer cells and silences MDR1 expression in xenograft model of human breast cancer, Iran J. Basic. Med. Sci. 18 (2015) 385–392.
[7] K.Y. Kim, S.H. Kim, S.N. Yu, S.K. Park, H.D. Choi, H.S. Yu, J.H. Ji, Y.K. Seo, S.C. Ahn, Salinomycin enhances doxorubicin-induced cytotoxicity in multidrug resistant MCF-7/MDR human breast cancer cells via decreased efflux of doxorubicin, Mol. Med. Rep. 12 (2015) 1898–1904.
[8] C.G. Zhang, W.J. Zhu, Y. Liu, Z.Q. Yuan, S.D. Yang, W.L. Chen, J.Z. Li, X.F. Zhou, C. Liu, X.N. Zhang, Novel polymer micelle mediated co-delivery of doxorubicin and P-glycoprotein siRNA for reversal of multidrug resistance and synergistic tumor therapy, Sci. Rep. 6 (2016) 23859.
[9] H. Ma, C.X. Deng, X.Y. Zong, Y.F. He, L.C. Cheng, Q. Fan, M.K. Shao, Y. Lin, C.Y. Zhao, G.R. Li, C. Zhang, Reversal of doxorubicin-resistance by delivering tetramethylprazine via folate-chitosan nanoparticles in MCF-7/ADM cells, Int. J. Clin. Exp. Med. 9 (2016) 5439–5448.
[10] A. Palmeira, M.H. Vasconcelos, A. Paiva, M.X. Fernandes, M. Pinto, E. Sousa, Dual inhibitors of P-glycoprotein and tumor cell growth: (Re)discovering thioxanthones, Biomed. Pharmacother. 83 (2012) 57–68.
[11] K. Takara, T. Sakaeda, K. Okumura, An update on overcoming MDR1-mediated multidrug resistance in cancer chemotherapy, Curr. Pharm. Design 12 (2006) 273–286.

[12] L.A. Garrett-Sinha, Review of Ets1 structure, function, and roles in immunity, Cell. Mol. Life Sci. 70 (2013) 3375–3390.
[13] L.A. Wilson, H. Yamamoto, G. Singh, Role of the transcription factor Ets-1 in cisplatin resistance, Mol. Cancer Ther. 3 (2004) 823–832.
[14] A. Khanna, K. Mahalingam, D. Chakrabarti, G. Periyasamy, Ets-1 expression and gemcitabine chemoresistance in pancreatic cancer cells, Cell. Mol. Biol. Lett. 16 (2011) 101–113.
[15] Z. Shaikhibrahim, N. Wernert, ETS transcription factors and prostate cancer: the role of the family prototype ETS-1, Int. J. Oncol. 40 (2012) 1748–1754.
[16] B.T. Kalet, S.R. Anglin, A. Handschy, L.E. O'Donoghue, C. Halsey, L. Chubb, C. Korch, D.L. Duval, Transcription factor Ets1 cooperates with estrogen receptor alpha to stimulate estradiol-dependent growth in breast cancer cells and tumors, PLoS One 8 (2013), e68815.
[17] M.D. Kars, O.D. Iseri, U. Gunduz, Drug resistant breast cancer cells overexpress ETS1 gene, Biomed. Pharmacother. 64 (2010) 458–462.
[18] N. Oda, M. Abe, Y. Sato, ETS-1 converts endothelial cells to the angiogenic phenotype by inducing the expression of matrix metalloproteinases and integrin beta(3), J. Cell. Physiol. 178 (1999) 121–132.
[19] M. Nakada, J. Yamashita, Y. Okada, H. Sato, Ets-1 positively regulates expression of urokinase-type plasminogen activator (uPA) and invasiveness of astrocytic tumors, J. Neuropathol. Exp. Neurol. 58 (1999) 329–334.
[20] J. Sampath, D.X. Sun, V.J. Kidd, J. Grenet, A. Gandhi, L.H. Shapiro, Q.J. Wang, G.P. Zambetti, J.D. Schuetz, Mutant p53 cooperates with ETS and selectively up-regulates human MDR1 not MRP1, J. Biol. Chem. 276 (2001) 39359–39367.
[21] J.R. Wei, Y. Zhou, G.Q. Jiang, D. Xiao, Silencing of ETS1 reverses adriamycin resistance in MCF-7/ADR cells via downregulation of MDR1, Cancer Cell Int. 14 (2014).
[22] X. Xu, W. Ho, X. Zhang, N. Bertrand, O. Farokhzad, Cancer nanomedicine: from targeted delivery to combination therapy, Trends Mol. Med. 21 (2015) 223–232.
[23] K.L. Nastiuk, J.J. Krolewski, Opportunities and challenges in combination gene cancer therapy, Adv. Drug Deliv. Rev. 98 (2016) 35–40.
[24] M.J. Mitchell, C.S. Chen, V. Ponmudi, A.D. Hughes, M.R. King, E-selectin liposomal and nanotube-targeted delivery of doxorubicin to circulating tumor cells, J. Control. Release 160 (2012) 609–617.
[25] R. Schiffelers, Anti-tumor efficacy of tumor vasculature-targeted liposomal doxorubicin, J. Control. Release 91 (2003) 115–122.
[26] P. Pradhan, J. Giri, F. Rieken, C. Koch, O. Mykhaylyk, M. Doblinger, R. Banerjee, D. Bahadur, C. Plank, Targeted temperature sensitive magnetic liposomes for thermo-chemotherapy, J. Control. Release 142 (2010) 108–121.
[27] L.A. Han, R.Q. Huang, J.F. Li, S.H. Liu, S.X. Huang, C. Jiang, Plasmid pORF-hTRAIL and doxorubicin co-delivery targeting to tumor using peptide-conjugated polyamidoamine dendrimer, Biomaterials 32 (2011) 1242–1252.
[28] A.M. Chen, M. Zhang, D.G. Wei, D. Stueber, O. Taratula, T. Minko, H.X. He, Co-delivery of doxorubicin and Bcl-2 siRNA by mesoporous silica nanoparticles enhances the efficacy of chemotherapy in multidrug-resistant cancer cells, Small 5 (2009) 2673–2677.
[29] D. Cheng, N. Cao, J. Chen, X. Yu, X. Shuai, Multifunctional nanocarrier mediated co-delivery of doxorubicin and siRNA for synergistic enhancement of glioma apoptosis in rat, Biomaterials 33 (2012) 1170–1179.
[30] W. Chen, Y. Yuan, D. Cheng, J. Chen, L. Wang, X. Shuai, Co-delivery of doxorubicin and siRNA with reduction and pH dually sensitive nanocarrier for synergistic cancer therapy, Small 10 (2014) 2678–2687.
[31] W. Wei, P.-P. Lv, X.-M. Chen, Z.-G. Yue, Q. Fu, S.-Y. Liu, H. Yue, G.-H. Ma, Codelivery of mTERT siRNA and paclitaxel by chitosan-based nanoparticles promoted synergistic tumor suppression, Biomaterials 34 (2013) 3912–3923.
[32] D.-W. Dong, B. Xiang, W. Gao, Z.-Z. Yang, J.-Q. Li, X.-R. Qi, pH-responsive complexes using prefunctionalized polymers for synchronous delivery of doxorubicin and siRNA to cancer cells, Biomaterials 34 (2013) 4849–4859.
[33] J. Shen, Q. Wang, Q. Hu, Y. Li, G. Tang, P.K. Chu, Restoration of chemosensitivity by multifunctional micelles mediated by P-gp siRNA to reverse MDR, Biomaterials 35 (2014) 8621–8634.
[34] Q.L. Hu, Q.Y. Jiang, X. Jin, J. Shen, K. Wang, Y.B. Li, F.J. Xu, G.P. Tang, Z.H. Li, Cationic microRNA-delivering nanovectors with bifunctional peptides for efficient treatment of PANC-1 xenograft model, Biomaterials 34 (2013) 2265–2276.
[35] Q.D. Hu, H. Fan, Y. Ping, W.Q. Liang, G.P. Tang, J. Li, Cationic supramolecular nanoparticles for co-delivery of gene and anticancer drug, Chem. Commun. 47 (2011) 5572–5574.
[36] B. Landry, H.M. Aliabadi, A. Samuel, H. Guel-Uludag, X. Jiang, O. Kutsch, H. Uludag, Effective non-viral delivery of siRNA to acute myeloid leukemia cells with lipid-substituted polyethylenimines, PLoS One 7 (2012), e44197.
[37] Y. Zhou, C. Zhang, W. Liang, Development of RNAi technology for targeted therapy - a track of siRNA based agents to RNAi therapeutics, J. Control. Release 193 (2014) 270–281.
[38] Y. Yang, D. Pan, K. Luo, L. Li, Z. Gu, Biodegradable and amphiphilic block copolymer-doxorubicin conjugate as polymeric nanoscale drug delivery vehicle for breast cancer therapy, Biomaterials 34 (2013) 8430–8443.
[39] D. Szklarczyk, A. Franceschini, S. Wyder, K. Forslund, D. Heller, J. Huerta-Cepas, M. Simonovic, A. Roth, A. Santos, K.P. Tsafou, M. Kuhn, P. Bork, L.J. Jensen, C. von Mering, STRING v10: protein-protein interaction networks, integrated over the tree of life, Nucleic Acids Res. 43 (2015) D447–D452.
[40] H. Fan, Q.D. Hu, F.J. Xu, W.Q. Liang, G.P. Tang, W.T. Yang, In vivo treatment of tumors using host-guest conjugated nanoparticles functionalized with doxorubicin and therapeutic gene pTRAIL, Biomaterials 33 (2012) 1428–1436.
[41] J. Li, C. Yang, H. Li, X. Wang, S.H. Goh, J.L. Ding, D.Y. Wang, K.W. Leong, Cationic supramolecules composed of multiple oligoethylenimine-grafted beta-cyclodextrins threaded on a polymer chain for efficient gene delivery, Adv. Mater. 18 (2006) 2969–2974.
[42] N. Taulier, T.V. Chalikian, gamma-cyclodextrin forms a highly compressible complex with 1-adamantanecarboxylic acid, J. Chem. Phys. B 112 (2008) 9546–9549.
[43] C. Sanson, C. Schatz, J.F. Le Meins, A. Soum, J. Thevenot, E. Garanger, S. Lecommandoux, A simple method to achieve high doxorubicin loading in biodegradable polymersomes, J. Control. Release 147 (2010) 428–435.
[44] G. Lin, W. Zhu, L. Yang, J. Wu, B. Lin, Y. Xu, Z. Cheng, C. Xia, Q. Gong, B. Song, H. Ai, Delivery of siRNA by MRI-visible nanovehicles to overcome drug resistance in MCF-7/ADR human breast cancer cells, Biomaterials 35 (2014) 9495–9507.
[45] L. Zhang, H. Xiao, J. Li, D. Cheng, X. Shuai, Co-delivery of doxorubicin and arsenite with reduction and pH dual-sensitive vesicle for synergistic cancer therapy, Nano 8 (2016) 12608–12617.
[46] G. Stokman, Y. Qin, Z. Racz, P. Hamar, L.S. Price, Application of siRNA in targeting protein expression in kidney disease, Adv. Drug Deliver. Rev. 62 (2010) 1378–1389.
[47] T. Yu, X. Liu, A.L. Bolcato-Bellemin, Y. Wang, C. Liu, P. Erbacher, F. Qu, P. Rocchi, J.P. Behr, L. Peng, An amphiphilic dendrimer for effective delivery of small interfering RNA and gene silencing in vitro and in vivo, Angew. Chem. 51 (2012) 8478–8484.
[48] X. Liu, J. Zhou, T. Yu, C. Chen, Q. Cheng, K. Sengupta, Y. Huang, H. Li, C. Liu, Y. Wang, P. Posocco, M. Wang, Q. Cui, S. Giorgio, M. Fermeglia, F. Qu, S. Pricl, Y. Shi, Z. Liang, P. Rocchi, J.J. Rossi, L. Peng, Adaptive amphiphilic dendrimer-based nanoassemblies as robust and versatile siRNA delivery systems, Angew. Chem. 53 (2014) 11822–11827.
[49] G. Szakacs, J.K. Paterson, J.A. Ludwig, C. Booth-Genthe, M.M. Gottesman, Targeting multidrug resistance in cancer, Nat. Rev. Drug Discov. 5 (2006) 219–234.
[50] S. Wang, J. Lin, T. Wang, X. Chen, P. Huang, Recent advances in photoacoustic imaging for deep-tissue biomedical applications, Theranostics 6 (2016) 2394–2413.
[51] C. Liu, X. Gong, R. Lin, F. Liu, J. Chen, Z. Wang, L. Song, J. Chu, Advances in imaging techniques and genetically encoded probes for photoacoustic imaging, Theranostics 6 (2016) 2414–2430.
[52] L. Zheng, T. Qi, D. Yang, M. Qi, D. Li, X. Xiang, K. Huang, Q. Tong, MicroRNA-9 suppresses the proliferation, invasion and metastasis of gastric cancer cells through targeting cyclin D1 and Ets1, PLoS One 8 (2013), e55719.
[53] R. Wang, Y. Ma, D. Yu, J. Zhao, P. Ma, miR-377 functions as a tumor suppressor in human clear cell renal cell carcinoma by targeting ETS1, Biomed. Pharmacother. 70 (2015) 64–71.
[54] N. Ma, F. Chen, S.-L. Shen, W. Chen, L.-Z. Chen, Q. Su, L.-J. Zhang, J. Bi, W.-T. Zeng, W. Li, X.-H. Huang, Q. Wang, MicroRNA-129-5p inhibits hepatocellular carcinoma cell metastasis and invasion via targeting ETS1, Biochem. Biophys. Res. Commun. 461 (2015) 618–623.
[55] W. Wei, Z. Hui, H. Fu, Y. Tie, H. Zhang, Y. Wu, X. Zheng, MicroRNA-1 and microRNA-499 downregulate the expression of the ets1 proto-oncogene in HepG2 cells, Oncol. Rep. 28 (2012) 701–706.

Supplementary Information

Targeting ETS1 with RNAi-based Supramolecular Nanoassemblies for Multidrug-Resistant Breast Cancer Therapy

Min Wu [a, b,1], Xingang Liu [a,1], Weihong Jin [b], Yongbing Li [a, b], Yang Li [a, b], Qinglian Hu [c], Paul K. Chu [b], Guping Tang [a,b,*], Yuan Ping [d,*]

[a] Institute of Chemical Biology and Pharmaceutical Chemistry, Zhejiang University, Hangzhou, 310028, P. R. China

[b] Department of Physics & Materials Science, City University of Hong Kong, Tat Chee Avenue, Kowloon, Hong Kong, China

[c] College of Biotechnology and Bioengineering, Zhejiang University of Technology, Hangzhou 310032, China

[d] School of Materials Science and Engineering, Nanyang Technological University, Singapore 639798, Singapore

E-mail: tangguping@zju.edu.cn (G.P.) or pingyuan7@gmail.com (Y. P.)

[1] These authors contributed equally to this work.

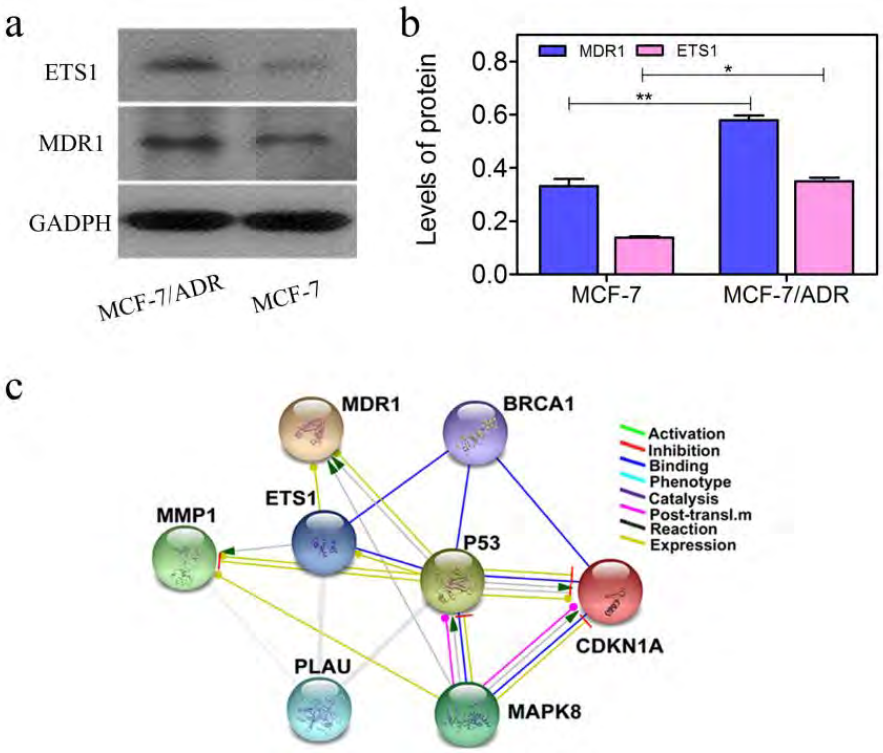

Fig. S1. (a)Western blot and (b)relative quantification analysis of ETS1 and MDR1 expression for MCF-7 and MCF-7/ADR cells. All data represent mean ± SD (n = 3). (Student t-test, *p < 0.05, **p < 0.01). (c) Protein-protein interaction (PPI) networks analysis of ETS1, MDR1 and relevant proteins calculated by STRING v10 software according to STRING protein interaction database.

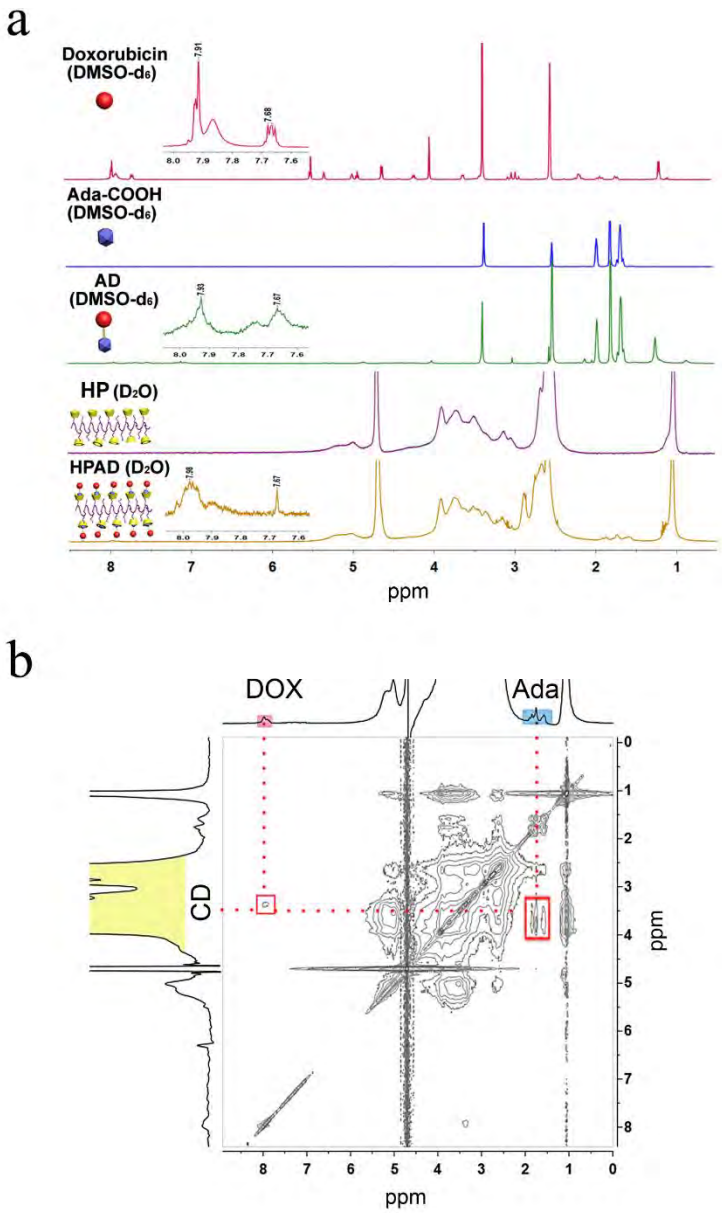

Fig. S2. (a) ^{1}H NMR spectra of DOX, Ada-COOH, AD，HP and HPAD. (b) 2D-NOESY NMR spectra of HPAD in D_2O.

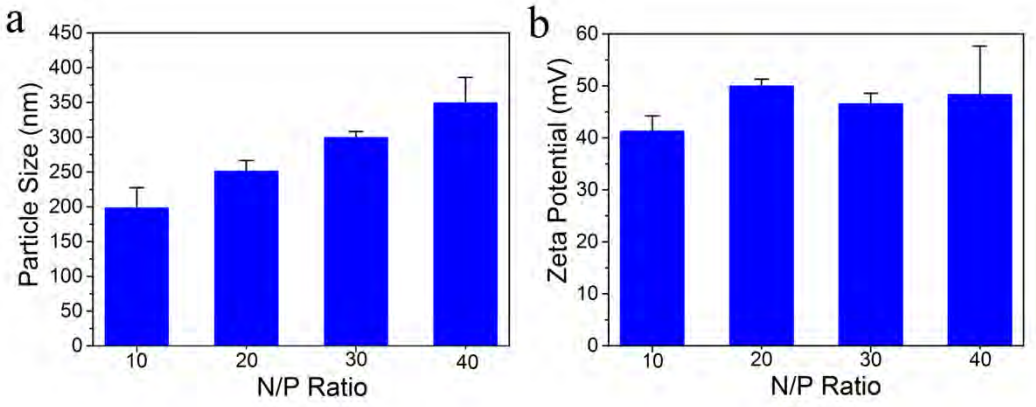

Fig. S3. (a) Particle size and (b) zeta potential of HPAD/siRNA complexes at various N/P ratios of 10, 20, 30 and 40.

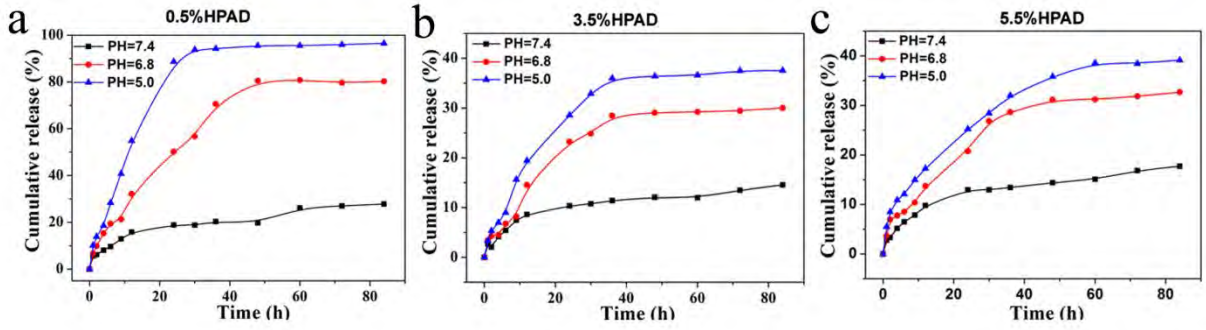

Fig. S4. Time-dependent cumulative release of DOX from HPAD with different drug loading ratio at different PH values.

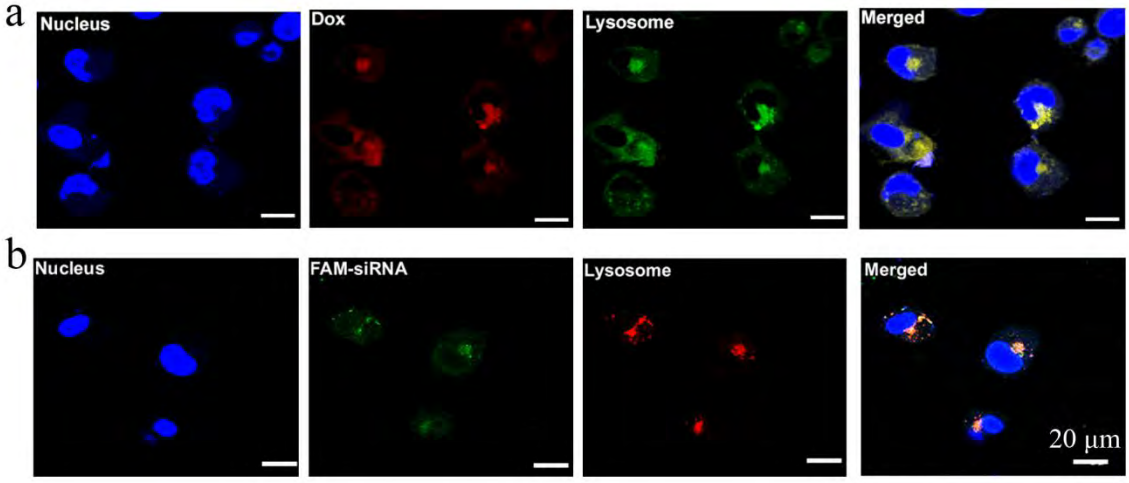

Fig. S5. Intracellular distributions of (a) HPAD and (b) HP/FAM-siRNA complexes in MCF-7/ADR cells after 4 h incubation. The concentration of DOX and FAM-siRNA was 5μM and 100 nM respectively. Cell nuclei were counterstained with DAPI (blue) and endolysosomes were stained by LysoTracker Red (green in a) and LysoTracker Green (red in b) respectively.

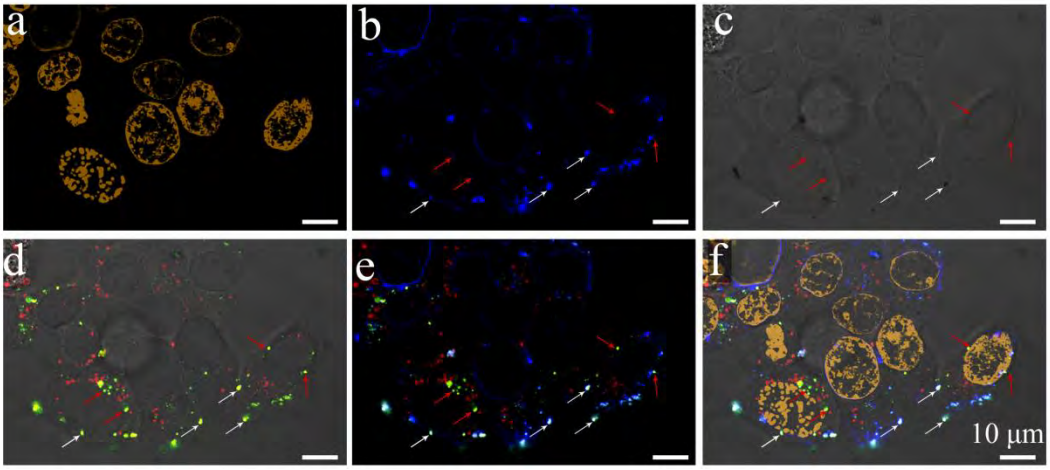

Fig. S6. CLSM images of MCF-7/ADR cells incubated with HPAD/FAM-siRNA complexes for 4 h. (a) nucleus counterstained with DAPI (dark yellow); (b) cell membrane counterstained with Alexa Fluor® 647 dye (blue); (c) Bright image; (d, e, f) Merged images: red means DOX and green means FAM-siRNA. Fluorescence was represented in pseudo color. The red arrow and the white arrow represented HPAD/FAM-siRNA complexes accumulated in lysosome and on the cell membranes, respectively.

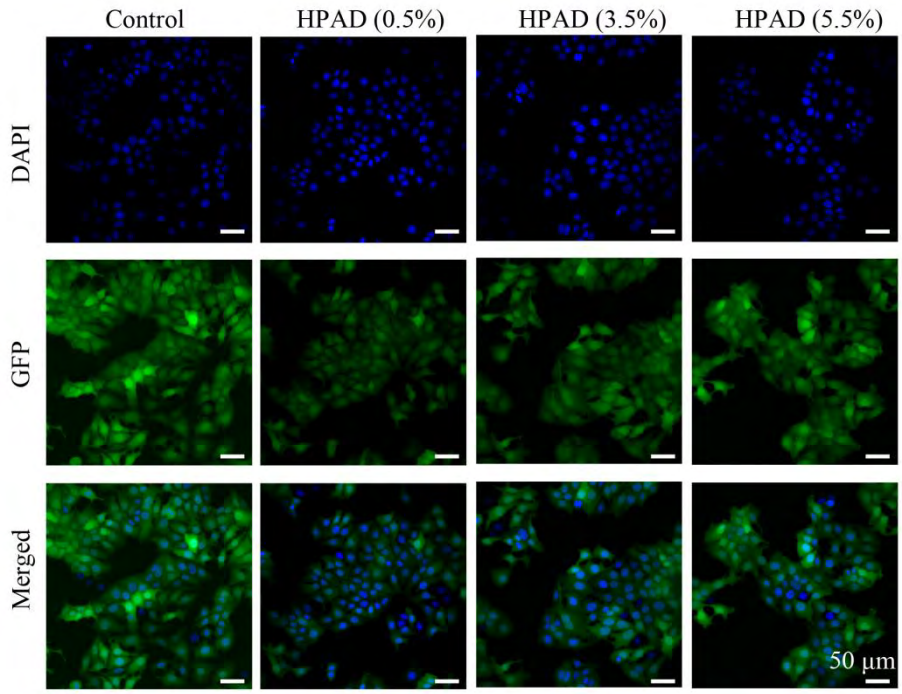

Fig. S7. CLSM of MCF-7/GFP cells treated with HPAD/siGFP complexes to investigate the effect of drug loading ratio on GFP silencing efficiency.

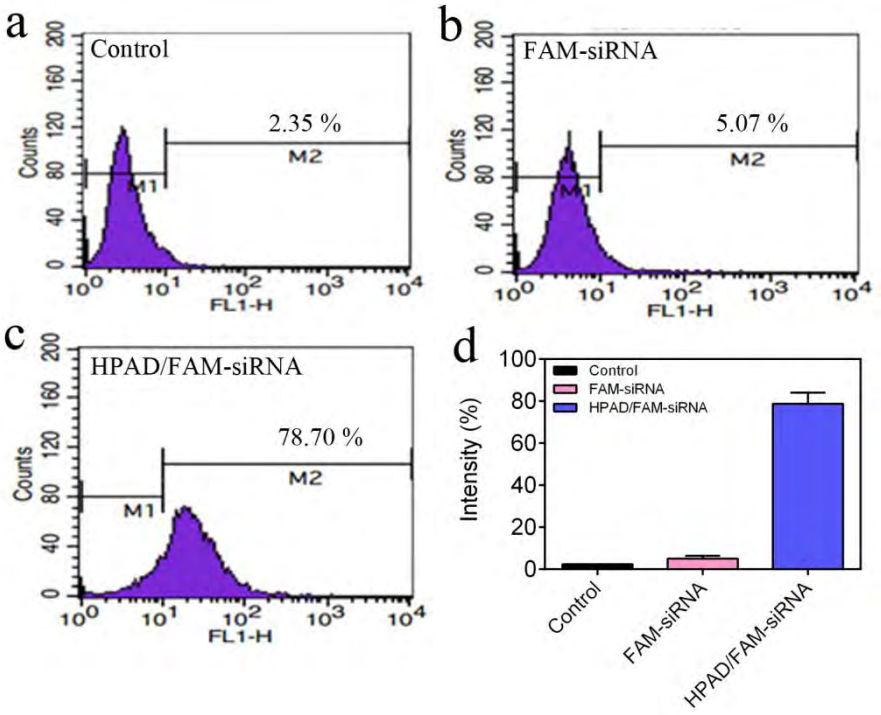

Fig. S8. Flow cytometry analyses of FAM-siRNA in MCF-7/ADR cells incubated with (a) HPAD, (b) free FAM-siRNA, (c) HPAD/ FAM-siRNA complexes to investigate the stability of siRNA in cellular uptake process. (d) Relative fluorescence intensity of FAM-siRNA in the above analyses.

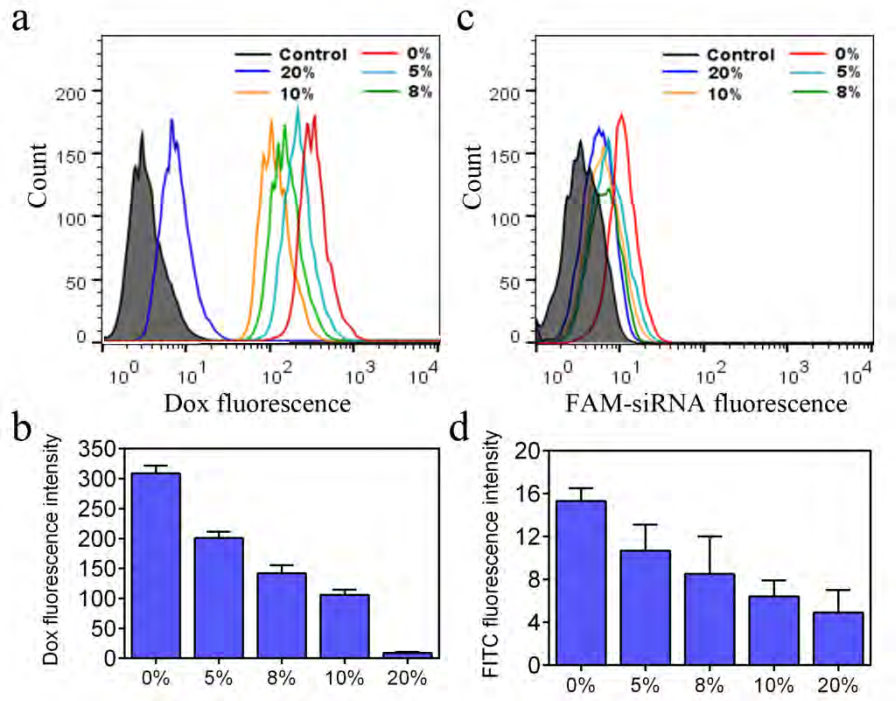

Fig. S9. Flow cytometry analyses of (a) DOX and (c) FAM-siRNA in MCF-7/ADR cells incubated with HPAD/ FAM-siRNA complexes for 4 h with DMEM containing different ratio of serum to investigate the effect of serum to the transfection efficiency. Fluorescence intensity of (b) DOX and (d) FAM-siRNA in the above analyses.

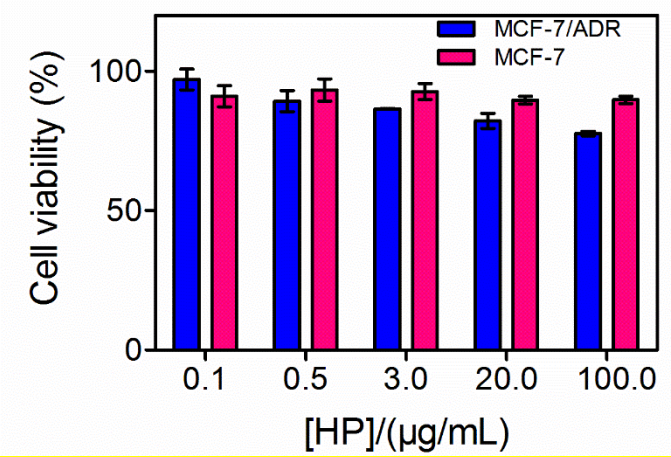

Fig. S10. Cell viability of MCF-7/ADR and MCF-7 cells after treated with HP for 48 h.

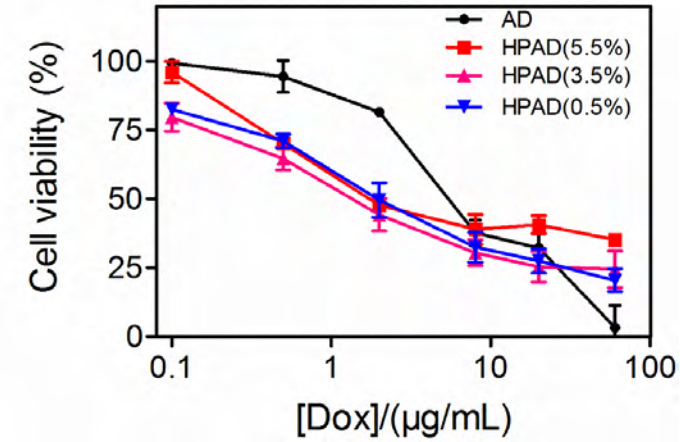

Fig. S11. Cell viability of MCF-7 cells after treated with HPAD with different DOX loading efficiency for 48 h.